WILEY-VCH

DOI: 10.1002/ ((please add manuscript number))
Article type: Review

Slow Photons for Photocatalysis and Photovoltaics

Jing Liu [a], Heng Zhao [a], Min Wu [a,], Benoit Van der Schueren [b], Yu Li [a,]*, Olivier Deparis [c], Jinhua Ye [d], Geoffrey Ozin [e], Tawfique Hasan[f] and Bao-Lian Su [a, b, g]**

Dr. J. Liu, Mr. H. Zhao, Prof. M. Wu, Prof. Y. Li.
State Key Laboratory of Advanced Technology for Materials Synthesis and Processing, Wuhan University of Technology, 122 Luoshi Road, 430070, Wuhan, Hubei, China;
E-mail: minwu@whut.edu.cn, yu.li@whut.edu.cn, baoliansu@whut.edu.cn

Prof. B. L. Su
State Key Laboratory of Advanced Technology for Materials Synthesis and Processing, Wuhan University of Technology, 122 Luoshi Road, 430070, Wuhan, Hubei, China; Laboratory of Inorganic Materials Chemistry (CMI), University of Namur, 61 rue de Bruxelles, B-5000 Namur, Belgium; Clare Hall, University of Cambridge, Herschel Road, Cambridge, CB3 9AL, United Kingdom.
E-mail: bao-lian.su@unamur.be

Dr. B. Van der Schueren
Laboratory of Inorganic Materials Chemistry (CMI), University of Namur, 61 rue de Bruxelles, B-5000 Namur, Belgium.

Prof. O. Deparis
Solid State Physics Laboratory, University of Namur, 61 rue de Bruxelles, B-5000 Namur, Belgium.

Prof. J. H. Ye
Research Unit for Environmental Remediation Materials, National Institute for Materials Science (NIMS),1-2-1 Sengen, Tsukuba, Ibaraki 305-0047, Japan.

Prof. G. A. Ozin
University of Toronto, Lash Miller Building Room 326 80 St. George Street,Toronto, Ontario M5S3H6, Canada

Dr. T. Hasan
Cambridge Graphene Centre, University of Cambridge, Cambridge, CB3 0FA, United Kingdom.

Keywords: Photonic Crystal, Slow Photon, Photocatalysis, Photovoltaics

Solar light is widely recognized as one of the most valuable renewable energy sources for the future. However, the development of solar energy technologies is severely hindered by poor energy conversion efficiencies due to low optical absorption coefficient and low quantum conversion yield of current generation materials. Huge efforts have been devoted to investigate new strategies to improve the utilization of solar energy. Different chemical and physical strategies have been used to extend the spectral range or increase the conversion efficiency of materials, leading to very promising results. However, these methods have now begun to reach their limits. What is therefore the next big concept that could efficiently be used to enhance light harvesting? Despite its discovery many years ago with the potential for becoming a powerful tool for enhanced light harvesting, the slow photon effect, a manifestation of light propagation control due to photonic structures, has largely been overlooked. This review presents theoretical as well as experimental progress on this effect, revealing that the photoreactivity of materials can be dramatically enhanced by exploiting slow photons. We predict that successful implementation of this strategy may open a very promising avenue for a broad spectrum of light energy conversion technologies.

1. Introduction

The year 2015 has been proclaimed as the **International Year of Light and Light-based Technologies**. Through this, the United Nations (UN) General Assembly have recognized the important role light-based technologies and applications have been playing in promoting sustainable development, taking up global energy challenges and improving quality of life. Indeed, light plays a vital role in our daily lives in the 21st century. Its successful exploitation is essential and warrants an interdisciplinary approach across many scientific fields.

Solar light is widely recognized as one of the most promising alternatives to fossil fuel-based energy sources. Significant endeavors have been devoted to the study, design and synthesis of novel materials able to convert solar energy into heat, electricity and chemical energy. In this regard, semiconductor materials have been extensively studied due to their capability of generating photo-excited electrons, which can, in turn, be used to generate electricity or induce chemical reactions. Therefore, irrespective of the way solar energy is exploited, light harvesting is always the primary concern as it determines the amount of photo-induced carriers. To date, solar energy technologies have mostly been developed for photocatalysis and photovoltaics. For example, perovskite-based solar cells have attracted a huge interest due to high conversion efficiency; above 20% with small laboratory-level cells and 11-13% with small module-level cells.[1] Indeed, the highest reported power conversion efficiency (PCE) of perovskite solar cell (27.6%) is a new record for single-junction solar cells under 1 sun illumination.[2] On the other hand,

polycrystalline chalcopyrite $Cu(In,Ga)(Se,S)_2$ (CIGS) solar cells have yielded the highest reported PCE of 21.7% [2]. In spite of the huge strides made in photovoltaics technologies, their efficiency remains lower than expected. For instance, the theoretical maximum PCE of Cu_2ZnSnS_4 is 30%[3] while the practical maximum is only 12.7%,[4] partly due to the low optical absorption coefficient and quantum conversion efficiency of the material. Innovative concepts boosting the development of new materials and new processes are the only solution to address the present situation.

In general, the methods used to enhance light harvesting can be categorized depending on whether they belong to one of the two following approaches. The first one is to enlarge the spectral region of the optical response of the semiconductor while the second one is to manipulate light in order to enhance its interaction with the semiconductor. The first approach has many options, which we describe hereafter. The semiconductors commonly adopted in photocatalysis applications, such as TiO_2 or ZnO, absorb mainly UV light due to their wide electronic bandgap. Since UV light represents only ~4% of the solar radiation on Earth, [5, 6, 7, 8] most of the solar energy is therefore not exploited, reducing the efficiency of light harvesting technologies based on these semiconductors. In order to increase the range of exploitable energy spectrum, several techniques have been implemented.[9] One technique is to dope the semiconductor with various transition metal cations in order to shift the optical absorption edge to the visible spectrum.[10] However, the performance of these doped semiconductors in photocatalysis[11, 12, 13] and photovoltaics[5, 14] has been found to

decrease over time, even in the UV region, due to thermal instability or increase in carrier recombination centers.[5, 10] Another technique involves doping with non-metallic ions such as fluorine,[15] nitrogen,[16] sulfur[17] and carbon[18] in order to decrease the electronic bandgap of the semiconductor. These dopant atoms enter the lattice and substitute oxygen, shifting the optical absorption edge to lower photon energies.[15, 19] The photoreactivity is generally enhanced due to higher light harvesting in the visible region[20]. However, it has been reported that the photoreactivity decreases in certain cases due to the lower redox potential of the photogenerated electrons and holes. [13] The third technique relies on the plasmonic effect, which has been recently introduced in solar energy applications and has attracted much attention.[13, 21, 22, 23] Noble metal nanoparticles such as Au[23, 24] and Ag[25, 26] can be incorporated into semiconductors. Their localized surface plasmon resonance improves the light harvesting capability of the nanocomposite. The fourth technique involves sensitizing wide bandgap semiconductors with ruthenium complex,[27] organic dyes,[28, 29, 30] quantum dots[31] and narrow bandgap semiconductors.[32, 33] The general idea is to use these sensitizers in order to absorb visible light and then transfer the photogenerated carriers to the wide bandgap semiconductors. A few other approaches have also been recently explored. For example, organometal halide perovskite materials have been used in solar cells, leading to increased efficiencies of up to 20%.[34, 35, 36] Also, infrared-to-ultraviolet up-conversion luminescence agents such as Y_2O_3:Yb^{3+}, Tm^{3+}, α -$NaYF_4$:Yb,Tm…[37, 38] have been introduced into semiconductors. Up-conversion luminescence is a

process through which multiple photons of lower energy are sequentially absorbed and eventually converted into one emitted photon of higher energy.[37, 38] These high energy photons can then generate carriers in the wide bandgap semiconductor.[39] The second approach for improving interaction of light with the semiconductor involves manipulation of light propagation in various material structures. For instance, multiple scattering[40, 41] can be used to allow more photons to be absorbed under a given light incidence condition. Random scattering by large particles[42] or spherical voids[43] has also been applied in dye-sensitized solar cells. Besides, hierarchically structured porous materials provide interconnected porosity at different length scales, which are very favorable for light harvesting. [44] The use of opal and inverse opal (IO) structures, a kind of photonic crystals with periodicity in structure, have attracted much attention due to their structure effect in light harvesting which we will discuss in following sections. In addition to opal and inverse opal (IO) structures, light harvesting enhancement, in a broader sense, may also be achieved by using other photonic structures, such as photonic crystal fibers [45, 46, 47], or micro/nano-prisms [48, 49, 50, 51] and lenses [52, 53]. Photonic crystals, however, are the best material ever devised for light manipulation. In the next section, we will focus on their potential use for the improvement of light harvesting.

2. Photonic crystals and slow photons.

Learning from nature can provide significant insights on the development of new physical concepts for light harvesting improvement. In nature, in addition to mineral opals, there are many species of butterflies, weevils, beetles and so on and so forth which exhibit vivid, iridescent colors due to internal or external structures, beside colors due to chemical pigments (**Figure 1**).[54] Today, it is well known that these structural colors originate from thin layers, layer stacks or more elaborated photonic crystal (PC) periodic structures.

Butterflies are one of the most colorful animal species. There are two mechanisms explaining their very diverse wing colors: pigmentary and structural colorations.[55, 56, 57, 58] The pigmentary coloration arises from chemical pigments which absorb light in certain wavelength ranges while the structural coloration is due to the interference of light travelling in the intricating and nanostructured wing, which results in strong, spectrally selective reflectance.[55, 59] **Figure 1b** and **1c** presents SEM images of the forewing and hindwing of *Gonepteryx Cleopatra* butterfly, in which the upper side of the scales covering the wings is composed of a stack of lamellae formed by folded densely packed, longitudinal ridges.[55] Within the lamellar stack, which is raised parallel to the scalesurface, individual lamellae are tilted with respect to the scale surface. These lamellae stacks form regular periodic multilayers, which create iridescent color.[57, 60] Wilts's work indicates that the number of the lamellae, the tilt angle and the thickness of each layer varies among the species and so does the reflectance spectrum.[55] All the reflectance spectra shown in **Figure 2a** have similar features: a distinct reflectance band with variable amplitude in the shorter wavelength

range which is due to the multilayered ridges forming an interferential reflector; a reflectance minimum caused by the pigment absorbing the incident light; a high reflectance plateau in the longer wavelength range which is due to the scattering of the incident light[55] Thus the species-characteristic wing colors are produced by pigment absorption, scattering and wavelength-selective multilayer reflection.[60, 61, 62] In addition, in all the studied species in this work,[55] the reflectance peak-wavelength shows a clear -dependence on the light incidence angle (**Figure 2b**), typical of multilayered structures where the reflectance peak wavelength decreases with increasing light incidence angle. The study of reflectance spectra reveals that the iridescent color of the butterfly wing is related to the reflectance peak wavelength of its nanostructured wing (**Figure 3**). [62, 63]

Photonic crystals are periodic ordered structures composed of two constituents, one with a low refractive index (RI) and the other with a high RI. The spatial periodicity in the RI creates a photonic band gap (PBG) or stopband,[64] analogous to the electronic band gap in semiconductor materials. The PBG forbids certain wavelengths to propagate in the photonic crystal (**Figure 4**).[64] The periodic RI structure affects the motion of photons in the same way as ionic lattice affects the motion of electrons in solids[64]. As illustrated in **Figure 4,** on the lower photon energy edge (red edge) of the photonic band gap, the light standing wave peaks are primarily localized in the high RI dielectric sections of the photonic crystal, whereas on the higher photon energy edge (blue edge), they are localized in the low RI dielectric sections. This mechanism provides photonic crystals with the capability of manipulating light in a

unique manner. Most importantly, on both the blue and red edges of the photonic band gap, vanishing group velocity is observed.[65] These photons with reduced group velocity are termed as “slow photons” (or “slow light”).[65, 73]

In general, the red-edge slow photons are believed to have relatively more practical applications as light intensity, in this case, is mainly localized in the high RI regions of the PC structure (e.g. the skeleton of an inverse opal) as revealed in photocatalysis and photovoltaic devices.[66, 67, 68, 69] Most recently, Deparis and Su demonstrated, through rigorous couple wave analysis simulations of light intensity distribution in inverse opals, that the blue-edge slow photons are also able to enhance light harvesting. The blue-edge enhancement has also experimentally been demonstrated by Su and others[70, 71, 72]. However, the comparison of photocatalytic enhancement between red-edge and blue-edge slow photons has rarely been experimentally investigated and remains a controversial issue, to the best of our knowledge. In spite of this, the slow photon effect in photonic crystals continues to attract huge interest.

The formation of slow photons arises from the interaction between the wave packet reflected by the photonic band gap and the non-reflected (i.e. transmitted) wave packet, at wavelengths outside but close to the gap. This interaction creates a stationary wave packet with a strongly reduced group velocity (equal to zero for an ideal PC) (**Figure 4**). The reduced group velocity implies a longer lifetime of the photons and a largely increased optical path length of the light wave in the material, promoting the interaction between light and material. Slow light has therefore an immense potential for light harvesting enhancement in solar energy applications.[73, 74]

In the seventies, Bykov[75] and Ohtaka[76] theoretically studied the peculiarity of photonic crystals and the formation of a photonic band gap. In the early nineties, Yablonovich's work on the synthesis of artificial photonic crystals[77] drew much interest in these new materials. Since then, photonic crystals have been synthesized by simple chemical methods.[78, 79, 80, 81, 82, 83, 84] Among them, inverse opal type photonic crystals have been extensively used in photocatalysis due to their open structure.[85, 86] Indeed, the advantages of such ordered macroporous skeleton structures in terms of enhanced light-matter interaction (and thus enhanced optical absorption and photochemical reactions) suggest that photonic crystals can play an important role in improving photocatalytic activity.[87, 88, 89] However, the observed photoreactivity enhancement is often attributed to the more efficient mass transport in the macroporous structure of the material and the slow photon effect is sometimes claimed but without evidence. Only recently, researchers have begun to exploit the slow photon effect in solar energy applications. For instance, Ozin's group pioneered the demonstration of photodegradation enhancement in TiO_2 inverse opals *via* the slow photon effect[79]. Mallouk's group observed light harvesting enhancement in dye-sensitized solar cells by coupling photonic crystals to semiconductor materials.[64] Also, Su's group theoretically and experimentally demonstrated correlations between the slow photon effect and the photocatalytic activity enhancement in inverse opals based on both TiO_2 and ZnO.[90, 91] Another possible application of the slow photon effect is in photoelectrochemical cells.[45, 52, 82] WO_3 photoanodes based on 3D-photonic crystals were fabricated by Ye's group.[66, 92] The authors found that

when the red-edge of the photonic band gap of WO_3 inverse opals overlapped with the WO_3 electronic absorption edge (E_g = 2.6-2.8 eV) the photocurrent intensity was increased by up to 100% under visible light irradiation compared to the intensity from a disordered porous WO_3 photoanode.[66]

Although the slow photon concept is very promising for light harvesting enhancement and thus for improving the efficiencies of solar cells and photocatalysts, its exploration remains a great challenge. This is partly due to the fact that the absorption enhancement due to slow photons in semiconductor materials can occur only if the wavelength at the photonic band red or blue edgematches the electronic excitation wavelength.[79] Moreover, preliminary studies in photocatalysis have mostly focused on the degradation of organic pollutants.[67, 80, 91, 93, 94] To date, only a few studies on the exploitation of the slow photon effect for photocatalytic water-splitting,[95, 96, 97] one of the most important solar energy conversion reactions for green fuel production, have been reported. In addition, the exploitation of the slow photon effect for the development of highly efficient solar cells has also been very limited.[1, 3, 4, 47, 98]

In this review article, we discuss both theoretically and experimentally the significance of the slow photon effect in light harvesting enhancement and the feasibility of its exploitation in applications,. The formation mechanism of slow photons is explained at first. We also give an introduction to the methods used to achieve the slow photon effect. Various applications of slow photons for an improved utilization of solar energy are then described. The feasibility of photoreactivity

enhancement due to slow photons is also highlighted in these applications. We then present our perspectives on this topic, concluding that slow photons have a strong and realistic potential to bring a step-change improvement in light harvesting through several strategies and is likely to attract a widespread attention in the near future.

2.1. The origin of the slow photon effect in photonic crystals

In the targeted solar energy applications, photons are absorbed by the semiconductor material and coupled with the photonic crystal structure. The basic idea is the following: if photons could reside in the material for a longer time, then the interaction between matter and light would be enhanced. A photonic crystal is characterized by its dispersion band curve, *i.e.* light frequency ω versus wavevector k, of which the Bloch modes near the photonic band gap edges are the focus here.[64, 99, 100, 101, 102, 103] In a photonic crystal of length L along the propagation direction, light travels in a Bloch mode with a lifetime τ given by $1/\tau = V_g/L + \alpha/(4\pi)(2\pi/L)^2 + \ldots$, where V_g is the group velocity of light ($V_g = d\omega/dk$) and α is the curvature of the Bloch mode dispersion curve ($\alpha = d^2\omega/dk^2$).[65] It is obvious that, at the minimal curvature point ($\alpha \sim 0$) which corresponds to vanishing group velocity ($V_g \sim 0$), the corresponding Bloch mode has the longest lifetime and for this reason, is termed as the "slow Bloch mode". Due to its very long lifetime, the slow Bloch mode interacts much more strongly with the material than other modes so that coupling of the incident light with that mode eventually leads to higher absorption.

In 1984, Asher's group discovered that a three-dimensional photonic crystal colloidal array of polystyrene spheres could reject light of certain wavelengths due to

Bragg scattering and band gap formation.[104, 105] In 2003, Mallouk's group found that the inverse opal type of photonic crystal can not only act as a dielectric mirror but also cause a significant change in dye absorbance, likely due to slow photons, which leads to enhancement of the light harvesting efficiency of dye-sensitized photoelectrodes[64]. In 2005, Miguez's group theoretically investigated the effect of photonic crystals in light harvesting enhancement and suggested that the propagation of slow photons could result in absorption enhancement.[106] **Figure 5a-c** shows SEM images of bilayer photonic crystal-nano TiO_2 photoeletrodes extracted from Ref 64. **Figure 5d** shows the calculated photonic band structure along the Γ-L direction for a dye-sensitized close-packed inverse opal TiO_2 faced-centered cubic structure. **Figure 5e** and **5f** present simulated reflectance and absorbance spectra at normal incidence, respectively, using the same parameters as in **Figure 5d**, while **Figure 5g** shows the effective group velocity (c/V_g). The reflectance and absorbance spectra of a non-structured dye-sensitized TiO_2 slab are also shown for comparison.

A reflection peak is observed (**Figure 5e**) at the wavelengths that are not allowed to propagate in the photonic crystal (corresponding to the band gap frequencies in **Figure 5d**). As a result of the finite size of the photonic crystal slab, evanescent waves within the band gap are coupled to the outside medium, causing reflection to be lower than unity, wider spectral width compared to the band gap width in **Figure 5d** and side lobes. Accordingly, a sharp enhancement of the absorbance is observed at both edges of the band gap, together with a deep reduction within the band gap (vertical dashed lines indicate the absorbance enhancement maxima in **Figure 5f**).

From the four plots in **Figure 5**, it is possible to make a quick analysis of the slow photon propagation in the photonic crystal. It is obvious that the absorbance maxima are positioned at both the higher (blue) and lower (red) energy edge of the band gap, which coincide with the maxima of the effective group velocity (C/V_g), *i.e.* the minima of the group velocity (V_g). This effect is the consequence of the band curvature in the dispersion relation of periodic dielectric media.[107] The light retardation, *i.e.* reduced group velocity (or increased effective group velocity), is the consequence of the slow photon formation at the edges of the photonic band gap and manifests directly its effect on the absorbance as an enhancement.

As suggested in the inset of **Figure 4** in the case of a one-dimensional photonic crystal, light is preferentially localized in the high refractive index regions of the photonic crystal at the red edge while it is primarily localized in the low refractive index regions at the blue edge.[64] This situation is analogous to the one encountered with electrons in semiconductors. When the photon energy is below the photonic band gap, the standing wave is localized preferentially in the high dielectric regions, here the semiconductor skeleton of the inverse opal (for instance, **Figure 6**). Meanwhile, when the photon energy is above the photonic band gap, the standing wave is more likely localized in the low refractive index regions (*i.e.* the air voids). It is obvious that the localization of light depends on the photon energy and this fact suggests that the high refractive index medium (*i.e.* the semiconductor) interacts more strongly with the light at the red edge than at the blue edge of the photonic band gap. In photoreaction processes, if the incident photon energy overlaps with the red edge of

the photonic band gap, the interaction between the light and the absorber medium is effectively enhanced by the slow photon propagation, resulting in a higher photo-conversion efficiency. However, a few cases showed that when the photon energy overlaps with the blue edge of the photonic band gap, the photonic crystal material also exhibits higher photo-conversion efficiency.[88, 108] Very recently, Deparis and Su *et al* theoretically investigated the origin of light harvesting enhancement in inverse opals due to the slow photon effect and revealed a previously overlooked yet important aspect of 1D photonic crystals: the fact that the blue edge photons can also experience enhanced absorption.[70] This theoretical result suggests that not only red but also blue edge tuning may lead to enhancement of absorption through resonant enhancement of electromagnetic field intensity due to the confinement of light. The enhancement by blue edge photons still calls for further theoretical and experimental investigations.

2.2 The synthetic methods of fabricating photonic crystals for slow photon applications

Theory of light propagation in photonic crystals has shown the feasibility of exploiting slow photons to photoreactions. However, the lack of scalability and controllability, cost and structural defects[93, 109] in natural photonic crystals prevents their practical usage. It is therefore necessary to develop appropriate methods to synthesize artificial photonic crystal structures for slow photon applications.

In order to benefit from light coming from any incident directions (*i.e.* omnidirectional illumination) a complete photonic band gap must be created. This

implies two conditions. The first one is that the contrast should be at least equal to 2.8 between the refractive indices of the two constitutive materials of the photonic crystal.[110] The second one is the utilization of a three-dimensional photonic crystal since only a three-dimensional structure can exhibit a complete band gap[111] though partial photonic band gaps can be observed in uni-, bi- and three-dimensional photonic crystals. The band gap width is dependent on the refractive indices of the constitutive materials, their volume fractions, and structural defects.[112, 113] Bragg's equation and Snell's law (modified for photonic crystals) allow calculating the central wavelength λ_{gap} of the photonic band gap of inverse opals cut along the (111) crystallographic direction:[112]

$$\lambda = 2d_{111}\sqrt{n_{eff}^2 - \sin^2\theta} \quad (1)$$

$$n_{eff} = f \cdot n_1 + (1 - f) \cdot n_2 \quad (2)$$

where d_{111} is the lattice constant, n_{eff} is the effective refractive index, n_1 is the refractive index of the higher refractive index material (here, semiconductor) and n_2 is the refractive index of the lower refractive index material (here, air), f is the compactness factor of the structure (*i.e.* volume fraction of the semiconductor material) and θ is the incidence angle of light (defined with respect to the normal to the crystal surface). In the case of touching spheres (f=0.26), d_{111}= ((2/3)D)$^{1/2}$ where D is the sphere diameter. Thus, by controlling the sphere diameter, the incidence angle of light, the volume fraction and the effective refractive index, the band gap wavelength can be tuned.

The synthesis of uni- and bi-directional photonic crystal structures is well documented and has already been used for industrial applications[114] while the synthesis of the most important three-dimensional structure is still under development as the quality and the cost are yet to be optimized. In 1991, Yablonovich's group reported the first artificial three-dimensional photonic crystal with a complete photonic band gap operating in the microwave region.[77] The authors fabricated the structure by direct drilling into a commercial, low-loss, dielectric material. Later, structures with complete PBG in the infrared region were demonstrated.[115] In 1998, another structure, termed as "woodpile" structure[116] was proposed and fabricated using standard microelectronics fabrication technology (standard lithographic techniques). Although the fabricated photonic crystal materials presented a complete photonic band gap in the IR range, the exaggerated cost from lithographic synthesis forbids the use of such structures in the wide range of applications envisaged for these materials. New methods of synthesis, relying on chemical approaches, were also subsequently adopted.[50, 66, 84, 117, 118] Using chemical synthesis methods, good quality materials were obtained based on a simple natural structure: the opal. However, synthesizing spheres of photoactive materials and assembling them in opals present challenges since the precise control over the sphere size, their mechanical stability and the assembly process cannot be easily achieved. Thus, the synthesis of opals lost attention while its replica, the so-called "inverse opal" (the structure resulting from the inversion of solid and hollow regions, with similar optical properties) attracted much interest.[70, 108, 119, 120, 121] To obtain an inverse opal structure, the first step

requires the synthesis of the spherical template particles (polystyrene,[67, 122] poly-methyl-methacrylate[123] or silica[124]) with controlled size and low polydispersity. In a second step, these spheres are assembled by various techniques such as sedimentation,[125] deposition,[126] self-assembly,[127] physical confinement[128] or emulsion templating.[129] In a third step, the interstices of the opal template structure are filled (**Figure 6**) via sol infiltration,[130, 131, 132] chemical vapor deposition (CVD) ,[130, 133] atomic layer deposition,[134, 135] co-assembly[134] or electrochemical filling of pores.[136, 137] Finally, the template is removed, *via* either calcination for polymeric spheres or hydrofluoric acid etching for silica spheres, in order to obtain the inverse opal structure. The schematic process of the inverse opal synthesis is shown in **Figure 6**, which also includes typical scanning electronic microscope (SEM) images of the opal (left) and inverse opal (right) structure assembled using silica spheres[138].

Photonic applications of inverse opals have demonstrated their well-preserved optical properties as photonic crystals.[139, 140] Since 2005, inverse opals have drawn massive attention in the environment[79, 141, 142] and energy[84, 85, 89] research and application fields due to the enhancement of photoreactions, the macropores for convenient mass transfer, the ordered structure for the “slow photon” effect, and in some cases the light-induced hydrophilic surface for intimate water contact. Indeed, the simplicity of the inverse opal synthesis method and the flexible control of the sphere size for tuning optical properties lay a solid experimental ground for exploiting the slow photon effect in solar energy applications.

3. The "slow photon" effect in photonic crystals for solar energy applications

3.1 Photocatalysis

Stimulated by its unique properties, the slow photon effect in photonic crystals is now widely exploited in solar energy related areas such as photocatalysis[83, 95, 142, 143] and solar cells,[66, 144, 145, 146, 147, 148] besides its conventional applications in lasers[149, 150, 151] and other optoelectronic applications [152, 153, 154, 155]. Among the applications mentioned above, as an environment-friendly technology, photocatalysis based on photonic crystal nanostructures has aroused much attention due to its efficient degradation rate of organic pollutants.[25, 91, 95, 142, 147, 156, 157]

For photocatalytic applications, pure semiconductors such as TiO_2, ZnO, Fe_2O_3 and their composites drove tremendous attention in recent years.[23, 156, 158, 159, 160, 161, 162] The most common semiconductor employed in photocatalysis is TiO_2[5] as it is non-toxic, inexpensive and stable during photochemical reactions.[163] Early results by Ozin's group[68, 79, 80, 93, 164] used a three-dimensional photonic crystal (inverse opal) and demonstrated optically amplified photocatalytic reactions by slow photon coupling.[79] For this purpose, inverse opals made of anatase nanocrystals and of different macropore sizes (denoted as i-nc-TiO_2-o) were synthesized in order to obtain different photonic stop band maximum positions.[79] **Figure 7b** shows the photonic stop band maxima with respect to the different macropore sizes. The shaded region indicates the irradiation wavelength used for photodegradation experiment with monochromatic light. The black and gray dashed curves are the extinction spectra of nanocrystalline TiO_2 and methylene blue, respectively. The vertical black arrows

point to the wavelength of the slow photons. It shows three distinct scenarios according to the samples: i) the photonic stop band overlaps the monochromatic irradiation wavelength, the case of 370-i-nc-TiO_2-o sample; ii) the slow photons at 370 nm overlap the red edge, the case of 345-i-nc-TiO_2-o sample; and iii) no photonic effect is observed, the case of 280-, 300-, 325-, 430-, and 500-i-nc-TiO_2-o samples. It is evident that the stop band maximum at 345 nm has its red edge overlapping the monochromatic irradiation wavelength, which could result in photocatalytic enhancement. **Figure 7c** shows the photodegradation rates of TiO_2 inverse opal, TiO_2 nanocrystalline for comaprison and mesoporous SiO_2 as the blank. The photocatalytic results indicated that the inverse opal with 345-nm stop band maximum had the highest photodegradation rate and therefore demonstrated that the direct coupling to the slow photons resulted in optically amplified photocatalytic reaction.

According to the Bragg's equation and the Snell's law in **Equation 1** and **2**, the photonic band gap maximum is affected by the light incidence angle. If the angle is increased, the band gap maximum is shifted to the blue (*i.e.* to shorter wavelengths). We note that when the above photocatalytic experiments[79] were carried out at increasing incident angles, the inverse opal with the photonic band gap maximum at 370 nm was observed to have a higher photoactivity than the one with the maximum at 345 nm. This was because the red edge of the photonic band gap of the former was blue-shifted to the irradiation wavelength, allowing higher photoreactivity due to slow photon coupling (**Figure 7d**). White light illumination at different incident angles was used to simulate real photocatalysis conditions with TiO_2 inverse opal films,[67, 90, 157],

which also demonstrates the tunable photocatalytic activity along with the slow photon effect.

The photocatalytic activity and the photonic structure optical properties have to be correlated in order to clearly demonstrate the effect of slow photons in the photocatalytic enhancement when the photonic band gap edge coincided with the electronic absorption band. Several factors need to be considered when the slow photon effect is expected to be dominant in photocatalysis enhancement. If the irradiation is white light instead of monochromatic light, strong reflectivity from the stop band will compete with the absorption experienced by slow photons.[79] Hence, a delicate system with a very specific response should be designed which should have suppressed reflectivity, while maintaining the photonic feature in order to allow the slow photon effect to be dominant in the photocatalysis enhancement.[67, 165] Ozin's group demonstrated such a system called here i-nc-TiO_2-o (inverse opals made from anatase nanocrystals and different macropore sizes). They found that the optimal stop band position of i-nc-TiO_2-o for degrading organic molecules under white-light irradiation was 300 nm with an enhancement factor of 2.3 in comparison with conventional nanocrystallineTiO_2.[79] When the photocatalytic reactions occur in the liquid phase, the refractive index contrast is decreased and the group velocity of slow photons is increased, leading to the reduction of the photocatalytic enhancement.[68] This can be overcome by increasing the filling fraction of titania in the inverse opal structure.[68] Indeed, after treating the titania inverse opal with TiF_6^{2-} to increase the titania wall thickness, the photocatalytic efficiency was increased (**Figure 8**).

Further research showed that using slow photons coupled with the electronic band gap of titania allowed 24.8% higher efficiency compared with the commercial P25 titania in photocatalytic activity for the degradation of 1,2-dichlorobenzene; **Figure 9**.[112] The photonic band gap of titania inverse opal (abbreviated as PBG-TiO_2) had an absorption at ~350 nm in the UV range while the commercial P25 presented no characteristic feature in the transmission spectrum. Under this condition, the PBG-TiO_2 was coupled with the electronic band gap of titania in order to facilitate the appearance of the slow photon effect (**Figure 9a**). As a result, the degradation of studied chemical 1,2-dichlorobenzene was enhanced in the PBG-TiO_2 through higher photocatalytic activity compared to commercial P25 titania (**Figure 9b**). Similar phenomenon was also observed previously.[161]

For photocatalytic remediation in environmental applications, the photochemical process occurs very often in aqueous solution.[166, 167] Thus, studying the slow photon effect in aqueous solution instead of air is more useful for photocatalysis applications. Su's group reported observation of the slow photon effect in aqueous solution by using TiO_2 inverse opal (abbreviated as TiO_2-IO) films for photodegradation of Rodamine B (RhB) dye pollutant in the aqueous phase.[90, 157] The slow photon effect of TiO_2-IO films in the photocatalytic degradation of RhB was revealed by tuning the incidence angle and the sphere sizes in the opal films (**Figure 10a** and **b**). In comparison with mesoporous TiO_2 (m-TiO_2) films obtained under the same conditions, the TiO_2-IO films demonstrated a much higher photocatalytic activity.[90] According to Equations 1 and 2, the increased incidence angle and the decreased

sphere size cause the shift of the photonic band gap towards shorter wavelengths. When the incident angle is zero, the TiO_2-IO-700 film (macropore size: 185 nm, calcined at 700°C) showed a better photocatalytic activity than the TiO_2-IO-800 film (macropore size: 165 nm, calcined at 800°C). However, with increasing incident angles, the photocatalytic activity of the TiO_2-IO-700 film decreased whilst that of the TiO_2-IO-800 film increased sharply. This tuning resulted in the alteration of the overlap between the photonic band gap edge and the TiO_2 absorption edge, which induces the slow photon effect, i.e. absoprtion enhancement. By contrast, the photocatalytic activities of the m-TiO_2-700 and m-TiO_2-800 with mesoporous structures remained unchanged little with the incident angle (**Figure 10d**), suggesting only no influence of incident angle tuning in mesoporous structures. Excellent agreement between experimental and theoretical reflectance spectra confirmed the high quality of the photonic crystal structure of the samples. (**Figure 11**).[90, 157] To the best of our knowledge, this work [90] was the first published report to explore the slow photon effect in aqueous phase, which could have important implications in waste water treatment.

Another common semiconductor for photocatalysis is ZnO which shows a better photocatalytic activity in azo-dye degradation due to its high solar radiation absorption efficiency, high exciton binding energy (60 meV) and high electron mobility (200 $cm^2\ V^{-1}\ s^{-1}$).[167, 168, 169] The wettability of the inverse opal film is also important when studying its photocatalytic activity because it affects the adsorption of liquids on the surface, liquid mobility and effective area of the solid-liquid

interface.[91] To the best of our knowledge, this work [91] was the first published report to demonstrate the slow photon effect in highly ordered, dense and continuous ZnO inverse opal films and the unique property of photoinduced change in surface wettability and hence, photocatalytic activity. Indeed, the surface wettability of these ZnO inverse opal films could be tuned from superhydrophobic to hydrophilic using UV-visible irradiation through photogenerated holes. These reacted with lattice oxygen to form surface oxygen vacancies, which ensured smooth progress of the photocatalytic reaction **(Figure 12a** and **b**).[91] The hierarchically porous and photonic crystal structure with the slow photon effect resulted in the highest photocatalytic activity at an incidence angle of $\theta = 40^\circ$ when compared to the ZnO film without the IO structure. It isinteresting to mention that it was observed that photons at blue edge can also play an important role in accelerating photocatalytic degradation of RhB. Moreover, our results suggested that slow photons at the red edge of photonic band gap lead to a higher photocatalytic enhancement than those at the blue edge. Therefore further investigation on the utilization of slow photons at both edges is required and could be a new route to promote performance enhancement in all light absorption related fields (**Figure 12c**).

In addition to these two semiconductors, researchers also observed slow photon effect in Fe_2O_3 IO film (**Figure 13**).[160] The 3D-ordered macroporous nanocrystalline Fe_2O_3 film exhibits very good photostability and 2.4 times stronger photocatalytic activity for photodegradation of crystal violet dye in presence of H_2O_2 under visible light compared to nanocrystalline α-Fe_2O_3 film without ordered macropores. The

much stronger photocatalytic activity and photostability of 3D-ordered Fe_2O_3 film was attributed to the better light harvesting by slow photons and more convenient mass transport through macropores in the IO. The PBG of 3D-ordered Fe_2O_3 film in crystal violet aqueous solution was changed from 631nm (in air) to 787nm as voids were filled by water, increasing thereby the effective refractive index according to **Equation 1** and **2**. Moreover, while the multiple scattering effects are expected to be isotropic, the effect of PBG on the photocatalytic activity depends on the incident angle. Thus, angle-dependent solid-state photodegradation experiment with monochromatic irradiation at 550 nm (slightly less than the electronic absorption band gap of Fe_2O_3: 2.2eV) was conducted in order to discriminate the effect of PBG on the photocatalytic activity from other multiple scattering effects. The result showed a 1.63 times enhancement of the photocatalytic activity when the incidence angle was tuned to 45°. This is because the energy of the slow photons near the red edge of PBG moved into the monochromatic irradiation window when the incidence angle was tuned.

Tuning the photonic bandgap edges through the adjustment of the IO structure (e.g. pore diameter) in order to match the dye absorbance is another way to exploit the slow photon effect, especially in photodegradation of organic dyes exhibiting a well-defined absorption peak. This enhancement can be attributed to the intensified dye photosensitization by the slow photon effect.[170] Meng and co-workers synthesized ZnO inverse opals with different pore diameters (ZnO-510, ZnO-600, ZnO-720 samples, where 510, 600 and 720 nm were their corresponding PBG

position) and utilized various kinds of dyes with different absorption peaks as probe molecules (such as methyl orange: MO, rhodamine B: RhB, methylene blue: MB, 4-chlorophenol: 4-CP) in order to study the influence of PBG position versus dye absorption peak on the photocatalytic activities.[170] The photonic band gap position was altered by tuning the pore sizes. As a result, the blue and red edges either overlapped or were far away from the probe molecule absorption peak. The rate constant for photocatalytic degradation of RhB and MB was decreased first and then increased when the pore size increased. However, as no adsorption was observed on the surface of the ZnO IOs for the probe MO and 4-CP molecules, mass transport became the key factor that resulted in the increase of the degradation rate constant with increasing pore sizes (**Figure 14b**).

Even though the photocatalytic activity of semiconductor IO structures can be amplified through the slow photon effect, pure semiconductors can only utilize solar light in certain wavelength ranges, such as the UV range. Also, the recombination of photo-generated electron-hole pairs causes a decrease in the photocatalytic activity.[171] With respect to these considerations, doping the pure semiconductor IO skeleton with metals as co-catalysts arouses tremendous attention and has been considered as a promising way for photocatalytic enhancement since it can prolong lifetime of photogenerated carriers by accelerating the separation of electrons and holes.[172] Moreover, certain noble metals such as Au, Ag, Cu can act as photosensitizers in order to improve the photocatalytic activity by local light intensity enhancement approaches such as Surface Plasmon Resonance (SPR). The excitation of SPR results

in collective oscillations of the free electrons and enhances the concentration of the photogenerated charge carriers.[13, 22, 25]

For example, higher hydrogen generation rate in photocatalytic water splitting was achieved in TiO_2 IO skeleton thanks to the slow photon effect, by promoting light absorption and generating more electron-hole pairs while Pt helped the separation of the photogenerated electron-hole pairs.[158] Titania IO has been also doped with gold.[142] The undoped inverse TiO_2 opals (denoted as i-TiO_2-o) and the gold-doped ones (denoted as i-Au-TiO_2-o) with centimeter-scale long-range ordering showed photocatalytic activities two- and five-fold higher than nanocrystalline TiO_2, respectively. This enhanced photocatalytic performance was attributed to the synergetic effect on light absorption caused by slow photons and by surface plasmon resonance of Au nanoparticles.[95, 142, 156] Zhang et al [95] constructed a TiO_2 bi-layer structure in which a vertical array of TiO_2 nanorods (abbreviated as TiO_2-NRPCs) were covered by a highly-ordered TiO_2 photonic crystal layer (abbreviated as TiO_2-PCs) through a template-assisted sol-gel process. Au/TiO_2 composite photoanodes were then constructed with such structures as skeletons supporting the plasmonic Au nanoparticles (NPs) (**Figure 15**). The photonic band gap of TiO_2-PCs was altered carefully in order to couple it with the SPR of Au nanoparticles. The purpose was to maximize light harvesting as well as to investigate the synergistic effects of plasmonic metal nanostructures and semiconductor photonic crystals on light harvesting and conversion efficiencies. The results indicated that the slow photon effect could be tuned to the SPR and subsequently influence the

solar-to-hydrogen efficiency in a specific wavelength region.[95] The calculated conversion efficiency approached 0.71% for the Au/TiO_2 NRPC (250) photoanode, which was designed to exhibit a slow photon effect in the SPR region (450–600 nm) of Au NPs. This tremendous enhancement was attributed to the optimized coupling of the slow photon effect and the surface plasmonic resonance of the Au NPs, as well as the photoelectrode design.[95]

In addition to noble metal loaded IO composite photocatalysts, coupling other semiconductors with photonic crystals offers a novel strategy to utilize slow photons in photocatalytic applications.[23, 161, 162, 173] The recent works made by Su's group on $BiVO_4$ nanoparticles[81] and ZnO quantum dots[174] which decorate three-dimensionally ordered macroporous (abbreviated as 3DOM) photonic crystal TiO_2 presented the combined positive effect of the semiconductor heterostructure and the photonic crystal structure for photocatalytic degradation. Besides the binary composites, Su et al [23] further reported on a ternary photocatalyst TiO_2-Au-CdS based on 3DOM TiO_2 which enhances the light absorption by utilizing the slow photon effect. The light absorption region was extended by CdS doping in combination with the SPR effect of the Au NPs. In this work, the ternary photocatalyst was designed to separate the photogenerated charge carriers and to promote the water splitting efficiency. The results showed that the H_2 generation rate of 3DOM TiO_2-Au-CdS photocatalytst under visible light irradiation was 13-fold higher than that achieved using the 3DOM TiO_2-CdS reference photocatalyst.[23] This work presented an excellent example of the combined effect of slow photons and SPR

in the light absorption enhancement by photonic crystals for water splitting applications.

Based on these very encouraging achivements of $BiVO_4$ nanoparticles (NPs) sensitized TiO_2 inverse opal structures for visible photocatalysis and ZnO quantum dots sensitized TiO_2 inverse opal structures for UV light phtotcatalysis, a new ternary nanocomposite $BiVO_4$ NPs/ZnO QDs/TiO_2 inverse opal structure has been prepared and showed much higher photocatalytic activity compared to ninary nanocomposites of $BiVO_4$ NPs/TiO_2-IO and ZnO QDs/TiO_2-IO and a symbiose effect of sensitization and slow photons. [174]

3.2 Photovoltaics

The slow photon effect, which results in the enhancement of solar light absorption, is also a novel and efficient technique for increasing the photoconversion efficiency of solar cells.[144, 148, 175, 176] Indeed, solar cells based on silicon IO with a high refractive index contrast attracted widespread attention because of the demonstration of a complete photonic bandgap and large scale materials synthesis.[175, 176] Takashi's group demonstrated that the inverse crystalline Si opal (abbreviated as i-cSi-o), with its three-dimensional open structure, has a comparable electrical conductivity to bulk crystalline Si. In addition, such a structure can effectively trap light via slow photons and/or prolong life time of minority charge carriers through inhibition of their recombination by the omnidirectional photonic band gap.[175, 177] In another work,[145] the authors evaluated the spectral response for the electrical properties of i-cSi-o with 600 nm and 280 nm sphere diameter templates and observed a slow photon enhanced

photoconductivity (**Figure 16**). As hydrogen plasma passivation (HPP) was used to decrease the grain-boundary potential barriers originating from Si dangling bonds, the lifetime of photogenerated carriers was improved in order to make the slow photon effect more obvious to observe. In fact, the results showed a large increase in the photoconductivity enhancement ratio, not only on the photonic bandgap edges but also within the photonic bandgap,[145] likely originating from structural imperfections of the millimeter size i-cSi-o samples.[175, 177] Considering that i-cSi-o have defects related to structural disorder,[177] it is quite remarkable that the enhancement of the internal quantum efficiency (IQE) by HPP was higher around the edges of photonic bandgaps even with such structural imperfections. This is indeed an encouraging indicator of the potential benefit of the slow photon effect in silicon photonic crystal photovoltaics.[145]

Another example of the usefulness of the slow photon effect for photovoltaics is the WO_3 photoanode based on 3D-photonic crystals.[66] The three dimensionally ordered WO_3 photonic crystals with a sphere template diameter of 260 nm (WO_3-260) produced 3-times higher photocurrent intensity as compared to the unpatterned WO_3 sample. Moreover, the WO_3-260 sample showed higher absorbance due to the much stronger interaction of light with the WO_3 matrix thanks to the slow light trapped in the WO_3 matrix by multiple scattering and diffraction. Therefore, as observed in the IPCE (Incident Photon to Current Efficiency) enhancement factor curves, the WO_3-260 sample exhibited selective photoelectric conversion efficiency enhancement in specific spectral regions. When the red-edge of the photonic band gap of WO_3 IOs

overlapped with the WO_3 electronic absorption edge at E_g = 2.6-2.8 *eV*, a maximum of 100% increase in photocurrent intensity compared to that in a disordered porous WO_3 photoanode was observed under visible light irradiation. (**Figure 17**).[66]

The slow photon effect has also been explored for the new generation of solar cells: dye-sensitized solar cells (DSSCs) and quantum dot-sensitized solar cells (QDSCs).[28, 31, 92, 98, 144, 146, 147, 176, 178, 179] Applications of the slow photon effect were demonstrated by matching the photonic band gap edge either to the semiconductor electronic band gap[31, 147] or to the absorption peak of the sensitizer.[144]

In the architecture of a dye-sensitized solar cell, a chemisorbed layer of dye generating charge carriers is usually sandwiched by a semiconductor oxide film (*i.e.* mesoporous TiO_2), and a liquid electrolyte for transport of electrons and holes.[28, 29, 148, 180] The main drawback of solar cells is the low optical absorption coefficient of the material in the red and near-infrared ranges.[30, 181] Several groups have worked on this issue using different approaches. One solution is to insert a highly scattering layer with large particles.[43] Although it enhances light harvesting, it renders the solar cell opaque. Another solution is to use IOs or porous Bragg stacks as photonic band gap layers.[64, 112, 148, 178] The selected structure is the multilayer system presented in **Figure 18**.[144] The difficulty in this method is to assemble the photonic band gap layer with the previously deposited mesoporous TiO_2 without compromising the optical quality. Different approaches have been used to achieve this.[182, 183, 184] Mallouk's work used a bi-layer structure by coupling a TiO_2 photonic crystal layer to a conventional film of TiO_2 nanoparticles. The IO photonic crystal aimed at

exploiting two enhancement mechanisms: the first one involves a dielectric mirror effect which causes significant light localization and the second one is the slow photon effect .[64] However, theoretical simulations showed that the absorption enhancement was primarily due to multiple internal scattering and not due to the slow photon effect.[104, 105] Therefore, the role of slow photons in dye-sensitized solar cells still remains controversial and requires further investigation.

The slow photon effect has also been demonstrated as a new method for enhancement of QDSC performance.[98, 147, 179, 185] Xiao's work revealed that the highly ordered SnO_2 IO structure can effectively reduce charge recombination and increase the open-circuit voltage (V_{oc}), the fill factor and thereby the cell performance. The optimum conversion efficiency of CdS/CdSe co-sensitized solar cells based on SnO_2 IO structure can reach to 4.37% under AM 1.5 (100mW/cm^2) illumination with a high V_{oc} of 700mV.[147] A similar work reported in Ref [146] also exploited slow photon in QDSCs. The authors fabricated TiO_2 IOs and unstructured nanocrystalline TiO_2 (nc-TiO_2) films which were both sensitized with CdSe QDs. By tuning the absorbance of CdSe (absorption **edges** at 600nm and 650nm) to match the red or the blue edges of the photonic band gap of TiO_2 IOs, a maximum average enhancement factor of 6.7 ± 1.6 at 640 nm (60 nm to the blue of theTiO_2-IO stop band gap center) was achieved with respect to nc-TiO_2 films with comparable amount of CdSe sensitizer.[163] The significant amplification in the light-to-current conversion efficiency was the result of the slow light effect powered by the photonic crystal environment in the QDSC.

Applications of the slow photon effect can also be expanded in the field of photoluminescence. Li et al [108] demonstrated up to 60.6 times enhancement in fluorescence for 2,4,6-trinitrotoluene (TNT) detection in optimized PCs compared to that of the control sample. The authors attributed this enhancement to a combination of the slow photon effect and the large surface area of the SiO_2-IO structure.[108] The quenching efficiency of the PC-based sensor reached 80% after exposure to TNT vapor for 300 s.[108] Another related application of the slow photon effect is the enhancement of photoluminescence of SiC through their optimized photonic crystal structures.[186] Indeed, large-scale fabrication of such SiC structures is expected to greatly extend industrial applications of PCs in harsh environments.[186]

4. Outlook

The slow photon effect has been demonstrated, both theoretically and experimentally in an unequivocal manner, to be a promising solution for increasing light absorption in semiconductors by extending the residence time of photons in the material. In practice, as illustrated in **Figure 19**, when the irradiation source, the electronic band gap of the material and either the red edge or the blue edge of the photonic band gap of the structure overlap in the frequency (wavelength) domain, slow photons are expected to produce a tremendous benefit for light harvesting. The irradiation brings photon energy to the structured material, the slow photons on the edges of the photonic band gap ensure a longer presence of that energy within the structure, and the electronic band gap allows the photon energy to be transferred into

electrons and holes. Coordination of these three phenomena is essential to extract the benefit of slow photons for solar energy harvesting.

Since the slow photon effect plays a significant role in light harvesting enhancement, as it has already been proven in TiO_2 and ZnO materials by numerous theoretical and experimental works, the most important question is: "what is the next research and development direction for slow photons?" To address this, three aspects should be considered: materials, structures and applications (see **Figure 20**).

4.1 Materials: The choice of the IO skeleton material should be extended to semiconductors with various electronic band gap energies such as oxides (CeO_2, Co_3O_4 and La_2O_3 etc), sulphides, nitrides and many kinds of metal salts. Hybrid materials are also interesting in this context. Semiconductors that absorb visible light directly will be more beneficial to solar energy utilization. Particular attention should be given to the applications of slow photons employing opals and IOs in aqueous medium (instead of air) because of the detrimental effect a lower refractive index contrast (RIC) has in photonic bandgap properties. Both theoretical[110] and experimental[187] studies suggest that the condition RIC>2 should be satisfied for an efficient slow photon effect. However, even for IOs with RIC~2, an enhancement factor of ~3 for light harvesting can be achieved.[87, 109, 110, 187] If the RIC between the semiconductor and the surrounding medium (which is also the medium filling the pores in an inverse opal) exceeds a certain value, an omnidirectional photonic bandgap is expected.[110] For the IO structure, a complete photonic bandgap is expected if the condition RIC>2.8 is satisfied. In this case, a very large depletion of

the photonic density of states, called pseudogap, can be achieved.[110, 188] Therefore, engineering appropriate materials composition in order to optimize RIC would be one of the key research direction in the field of slow photons for photocatalysis and photovoltaics.

4.2 Structures: The most common photonic crystal structures for utilizing slow photons are opals and inverse opals. The quality of these structures is the experimental ground that is required to observe and exploit the slow photon effect. It is critical to have a large number of photonic crystal layers and an excellent order or packing in order to really stand a chance of reducing the group velocity of light to the levels that really lead to significant slow photon effects. Galisteo-Lopez [189] systematically investigated the formation of the pseudogap associated with the (111) photonic crystal planes as a function of the thickness in the direction perpendicular to the planes using reflection and transmission measurements. The transmittance monotonically decreases as the thickness of the sample increases when the number of the sample layer is >30. Through the attenuation coefficient (obtained from the transmittance and the crystal thickness), the extinction length is estimated to be ~8 layers. This estimation requires further investigation. The method of synthesis and assembly of the structure should also be optimized. A study of the physical and chemical interactions between the bead (i.e. templating sphere) surface and the semiconductor material precursor would be an important step for the inversion of the opal template. In addition, it is crucial to ensure complete infiltration of the precursor in the spherical template interstices. Changing the size of beads and allowing the

choice of organic or inorganic precursor materials are necessary to tune the photonic and electronic band gap. In addition, surface defects formed during the synthesis, often regarded as detrimental, could be utilized to enhance the photon localization effect and bound to the story of slow photons.[109, 113, 187] Bottom-up gravity-induced self-assembly of submicrometer spheres into a face-centered cubic opal lattice is the most common and facile method to fabricate photonic crystals. However, defects such as stacking faults and dislocations are inherent to the as-fabricated three dimensional photonic crystals. These defects in the photonic crystal structure are responsible for an incomplete photonic bandgap, and therefore regarded as a unfavorable factor in theoretical studies. However, this structural disorder can be used to amplify photocatalytic activity in practical applications. Chen[93] adopted guest spheres 1.2 times larger than the host spheres to fabricate titania IOs. The results showed that the photocatalytic enhancement can be observed when the guest-host substitution fraction was as high as 0.4. The presence of disorder could significantly broaden the photonic bandgap, resulting in the appearance of the strong light localization reported by YA Vlasov.[187]

Inverse opal is not the only example of photonic crystal structure. The slow photon effect in a wood-pile structure and in a opal structure made of hollow spheres may bring new perspectives in the field.[83, 190] In addition, Bragg stacks and 1D photonic crystals composed of nanocrystals have recently drawn great attention due to their simpler structure, high quality synthesis and tunable color reflection.[191, 192, 193] Coloderro *et al* presented a fast, reliable method for fabricating nanoparticle-based 1D

photonic crystals[194]. The authors demonstrated periodic modulation of the refractive index by alternating SiO_2 and TiO_2 nanoparticles and introducing porosity in each layer. The potential of the Bragg stacks as optical sensing materials for chemical and biochemical analytes are enormous. Such structures would allow change of structural colors when infiltrated by solvents with different refractive indices, enabling molecular selectivity of the sensor,and thus opening widespread applications across various areas.[195, 196]

Constructing a single photonic crystal with different active materials and different pore sizes could enable absorption over a broader spectral range. This could enable a wide variety of applications and could potentially be an exciting new research direction.

Finally, a better understanding of the effect of the blue edge slow photons and the comparison with that the effect of red edge slow photons are also crucial for further development of this field.

4.3 Applications: Since the slow photon effect is induced by light propagating in a PC structure and since it aims to enhance light harvesting by the very same structure, it could be applied in all light-related applications including photo-reactions,[95, 197] optical sensors[82, 198] and photovoltaics[86, 199, 200, 201, 202]. Moreover, which photonic bandgap edge (blue or red) is more efficient in the slow photon effect still remains a controversial question. So far, scientific reports have concentrated predominantly on results obtained with the red edge of the photonic band gap while few have

demonstrated better results with the blue edge. This requires systematic and careful investigations.

Finally, the slow photon effect may not act alone in light harvesting. Indeed, multiple scattering in 3D ordered structures can induce multiple resonant modes and result in strong light localization, thereby also enhancing the interaction between light and matter for amplified chemical reactions. The authors of Ref. 106,165 reported on a homogeneous silica layer with different thicknesses on the surface of a TiO_2 photonic crystal film. The presence of the external dielectric silica layer greatly modified the optical properties due to the existence of photon resonant states. Compared to conventional photoelectrodes, Mallouk et al[64] achieved a 26% enhancement in photocurrent by coupling a thin film of dye-sensitized TiO_2 nanoparticles with titanium dioxide PC structures. In addition to the slow photon effect, the authors attributed this photocurrent enhancement to the stronger light absorption that the thin film provides through a modulation of the scattered light intensity. The thickness and refractive index of the surface defect in a photonic crystal greatly affect the optical absorption enhancement. This is useful e.g. for monitoring the deposition process of thin films. These results shed a light on coupling the slow photon effect with multiple scattering in PC structures, as it is shown here by building a mirror-like slab or film on the surface of the PC in order to amplify light absorption. Las but not least, contributions from other effects such as stop-band reflection[161] and surface plasmon resonance[95, 143, 156] will also make the slow photon effect an effective strategy to boost performance of future solar energy applications.

Acknowledgements

This work was realized in the frame of a program for Changjiang Scholars and Innovative Research Team (IRT_15R52) of the Chinese Ministry of Education. B. Van der Schueren acknowledges FRIA funding from the Fonds National de la Recherche Scientifique (FNRS). T. Hasan acknowledges support from a Royal Academy of Engineering Fellowship, B. L. Su acknowledges the Chinese Central Government for an "Expert of the State" position in the Program of the "Thousand Talents", the Chinese Ministry of Education for a Changjiang Scholar position at the Wuhan University of Technology, a Clare Hall Life Membership, University of Cambridge. This work is also financially supported by National Natural Science Foundation of China (Grant No.51502225), the Fundamental Research Funds for the Central Universities (2013-YB-024, 2014-IV-057), Hubei Provincial Natural Science Foundation (2015CFB516) and Self-determined and Innovative Research Funds of the SKLWUT (2015-ZD-7) and International Science &Technology Cooperation Program of China (ISTC-2015DFE52870). G.A.O. is a Government of Canada Research Chair in Materials Chemistry and Nanochemistry. Financial support for this work was provided by the Ontario Ministry of Research Innovation (MRI); Ministry of Economic Development, Employment and Infrastructure (MEDI); Ministry of the Environment and Climate Change; Connaught Global Challenge Fund; Natural Sciences and Engineering Research Council of Canada (NSERC).

Received: ((will be filled in by the editorial staff))

Revised: ((will be filled in by the editorial staff))

Published online: ((will be filled in by the editorial staff))

References

[1] F. Di Giacomo, A. Fakharuddin, R. Jose, T. M. Brown, *Energy Environ. Sci.* **2016**, *9*, 3007.
[2] (a) B. M. Kayes, H. Nie, R. Twist, S. G. Spruytte, F. Reinhardt, I. C. Kizilyalli, G. S. Higashi, presented at Photovoltaic Specialists Conference (PVSC), 37th IEEE, 27.6% conversion efficiency, a new record for single-junction solar cells under 1 sun illumination, 2011. (b) B. P. reinhard, S. Buecheler, A. N. Tiwari, *Sol. Energ. Mat. Sol. Cell*. **2013**, *119*, 287-290
[3] A. H. Pinto, S. W. Shin, E. S. Aydil, R. L. Penn, *Green Chem.* **2016**, *18*, 5814.
[4] J. Kim, H. Hiroi, T. K. Todorov, O. Gunawan, M. Kuwahara, T. Gokmen, D. Nair, M. Hopstaken, B. Shin, Y. S. Lee, *Adv. Mater.* **2014**, *26*, 7427.
[5] X. Chen, S. S. Mao, *Chem. Rev.* **2007**, *107*, 2891.
[6] L. Qi, J. Yu, M. Jaroniec, *Phys. Chem. Chem. Phys.* **2011**, *13*, 8915.
[7] T. Hisatomi, J. Kubota, K. Domen, *Chem. Soc. Rev.* **2014**, *43*, 7520.
[8] S. Sakthivel, B. Neppolian, M. V. Shankar, B. Arabindoo, M. Palanichamy, V. Murugesan, *Sol. Energ. Mat. Sol.C.* **2003**, *77*, 65.
[9] X. Chen, S. Shen, L. Guo, S. S. Mao, *Chem.Rev.* **2010**, *110*, 6503.
[10] W. Choi, A. Termin, M. R. Hoffmann, *J. Phys. Chem.* **1994**, *98*, 13669.
[11] K. E. Karakitsou, X. E. Verykios, *J. Phys. Chem.* **1993**, *97*, 1184.
[12] M. A. Abdullah, F. K. Chong, *Chem. Eng. J.* **2010**, *158*, 418.
[13] X. Li, J. Yu, J. Low, Y. Fang, J. Xiao, X. Chen, *J. Mater. Chem. A* **2015**, *3*, 2485.
[14] X. Yang, A. Wolcott, G. Wang, A. Sobo, R. C. Fitzmorris, F. Qian, J. Z. Zhang, Y. Li, *Nano Lett.* **2009**, *9*, 2331.
[15] J. C. Yu, J. Yu, W. Ho, Z. Jiang, L. Zhang, *Chem.Mater.* **2002**, *14*, 3808.
[16] R. Asahi, T. Morikawa, T. Ohwaki, K. Aoki, Y. Taga, *Science* **2001**, *293*, 269.
[17] T. Umebayashi, T. Yamaki, H. Itoh, K. Asai, *Appl. Phys. Lett.* **2002**, *81*, 454.
[18] L. Mai, C. Huang, D. Wang, Z. Zhang, Y. Wang, *Appl. Surf. Sci.* **2009**, *255*, 9285.
[19] H. Y. Xu, Y. C. Liu, R. Mu, C. L. Shao, Y. M. Lu, D. Z. Shen, X. W. Fan, *Appl. Phys. Lett.* **2005**, *86*, 1231071.
[20] W. Ho, J. C. Yu, S. Lee, *Chem. Commun.* **2006**, *10*, 1115.
[21] H. Zhou, L. Ding, T. Fan, J. Ding, D. Zhang, Q. Guo, *Appl. Catal.B: Environ.* **2014**, *147*, 221.
[22] J. Ran, J. Zhang, Yu, Jiaguo , J. Mietek, S. Qiao, *Chem. Soc. Rev.* **2014**, *43*, 7787.
[23] H. Zhao, M. Wu, J. Liu, Z. Deng, Y. Li, B.-L. Su, *Appl. Catal.B: Environ.* **2016**, *184*, 182.
[24] A. Furube, L. Du, K. Hara, R. Katoh, M. Tachiya, *J. Am. Chem. Soc.* **2007**, *129*, 14852.
[25] J. Xu, X. Xiao, A. L. Stepanov, F. Ren, W. Wu, G. Cai, S. Zhang, Z. Dai, F. Mei, C. Jiang, *Nanoscale Res. Lett.* **2013**, *8*, 731.
[26] P. Wang, B. Huang, X. Qin, X. Zhang, Y. Dai, J. Wei, M.-H. Whangbo, *Angew. Chem. Int. Ed.* **2008**, *47*, 7931.

[27] Z. Wang, C. Huang, Y. Huang, Y. Hou, P. Xie, B. Zhang, H. Cheng, *Chem.Mater.* **2001**, *13*, 678.
[28] A. Hagfeldt, G. Boschloo, L. Sun, L. Kloo, H. Pettersson, *Chem.Rev.* **2010**, *110*, 6595.
[29] M. Quintana, T. Edvinsson, A. Hagfeldt, G. Boschloo, *J. Phys. Chem. C* **2007**, *111*, 1035.
[30] B. O'regan, M. Grätzel, *Nature* **1991**, *353*, 737.
[31] J. Hensel, G. Wang, Y. Li, J. Z. Zhang, *Nano Lett.* **2010**, *10*, 478.
[32] H. Tada, Q. Jin, H. Nishijima, H. Yamamoto, M. Fujishima, S.-i. Okuoka, T. Hattori, Y. Sumida, H. Kobayashi, *Angew. Chem. Int. Ed.* **2011**, *123*, 3563.
[33] S. B. Rawal, S. Bera, D. Lee, D. J. Jang, W. I. Lee, *Catal.Sci.Technol.* **2013**, *3*, 1822.
[34] H. J. Snaith, *J. Phys. Chem. Lett.* **2013**, *4*, 3623.
[35] M. M. Lee, J. Teuscher, T. Miyasaka, T. N. Murakami, H. J. Snaith, *Science* **2012**, *338*, 643.
[36] J. M. Ball, M. M. Lee, A. Hey, H. J. Snaith, *Energy Environ. Sci.* **2013**, *6*, 1739.
[37] T. Li, S. Liu, H. Zhang, E. Wang, L. Song, P. Wang, *J. Mater.Sci.* **2010**, *46*, 2882.
[38] J. Shen, G. Chen, T. Y. Ohulchanskyy, S. J. Kesseli, S. Buchholz, Z. Li, P. N. Prasad, G. Han, *Small* **2013**, *9*, 3213.
[39] J. Silver, M. Martinez-Rubio, T. Ireland, G. Fern, R. Withnall, *J. Phys. Chem. B* **2001**, *105*, 948.
[40] Y. Zhang, J. Liu, G. Wu, W. Chen, *Nanoscale* **2012**, *4*, 5300.
[41] Y. Li, T. Kunitake, S. Fujikawa, *J. Phys. Chem. B* **2006**, *110*, 13000.
[42] A. Usami, *Sol. Energy Mater.Sol. C.* **1999**, *59*, 163.
[43] S. Hore, P. Nitz, C. Vetter, C. Prahl, M. Niggemann, R. Kern, *Chem. Commun.* **2005**, *15*, 2011.
[44] (a) M. H. Sun, S. Z. Huang, L. H. Chen, Y. Li, X. Y. Yang, Z. Y. Yuan, B. L. Su, *Chem. Soc. Rev.* **2016**, *45*, 3479. (b) Y. Li, Z. Y. Fu, B. L. Su, *Adv. Funct. Mater.* **2012**, *22*, 4634–4667
[45] D. Mogilevtsev, T. A. Birks, P. S. J. Russell, *Opt. Lett.* **1998**, *23*, 1662.
[46] A. Ortigosa-Blanch, J. C. Knight, W. J. Wadsworth, J. Arriaga, B. J. Mangan, T. A. Birks, P. S. J. Russell, *Opt. Lett.* **2000**, *25*, 1325.
[47] P. Reader-Harris, A. Di Falco, *ACS Photonics* **2014**, *1*, 985.
[48] B. B. Kale, J.-O. Baeg, K.-j. Kong, S.-J. Moon, L. K. Nikam, K. R. Patil, *J. Mater. Chem.* **2011**, *21*, 2624.
[49] M. Stavytska-Barba, M. Salvador, A. Kulkarni, D. S. Ginger, A. M. Kelley, *J. Phys. Chem. C* **2011**, *115*, 20788.
[50] A. P. Kulkarni, K. M. Noone, K. Munechika, S. R. Guyer, D. S. Ginger, *Nano Lett.* **2010**, *10*, 1501.
[51] K. Yao, M. Salvador, C.-C. Chueh, X.-K. Xin, Y.-X. Xu, D. W. deQuilettes, T. Hu, Y. Chen, D. S. Ginger, A. K. Y. Jen, *Adv. Energy Mater.* **2014**, *4*, 1400206.

[52] J. Y. Lee, B. H. Hong, W. Y. Kim, S. K. Min, Y. Kim, M. V. Jouravlev, R. Bose, K. S. Kim, I.-C. Hwang, L. J. Kaufman, C. W. Wong, P. Kim, K. S. Kim, *Nature* **2009**, *460*, 498.
[53] W. T. Xie, Y. J. Dai, R. Z. Wang, K. Sumathy, *Renew. Sust. Energy Rev.* **2011**, *15*, 2588.
[54] O. Deparis, J. P. Vigneron, *Mat. Sci. Eng. B* **2010**, *169*, 12.
[55] B. D. Wilts, P. Pirih, D. G. Stavenga, *J Comp Physiol A* **2011**, *197*, 693.
[56] A. R. Parker, *Mater. Today* **2002**, *5*, 26.
[57] R. A. Potyrailo, H. Ghiradella, A. Vertiatchikh, K. Dovidenko, J. R. Cournoyer, E. Olson, *Nat. Photon.* **2007**, *1*, 123.
[58] K. Liu, L. Jiang, *Nano Today* **2011**, *6*, 155.
[59] J. Zi, X. Yu, Y. Li, X. Hu, C. Xu, X. Wang, X. Liu, R. Fu, *PNAS* **2003**, *100*, 12576.
[60] V. Saranathan, C. O. Osujib, S. G. J. Mochrie, H. Noh, S. Narayanan, A. Sandy, E. R. Dufresne, R. O. Pruma, *PNAS* **2010**, *107*, 11676.
[61] Gérard Tayeb, B. Gralak, S. Enoch, *Opt. Photonics News* **2003**, *2*, 40.
[62] S. Kinoshita, S. Yoshioka, *Chemphyschem* **2005**, *6*, 1442.
[63] P. Vukusic, R. Sambles, J. Bertolotti, Wing scales cause light to diffract and interfere: morpho butterflies, http://www.asknature.org, 2008.
[64] S. Nishimura, N. Abrams, B. A. Lewis, L. I. Halaoui, T. E. Mallouk, K. D. Benkstein, J. van de Lagemaat, A. J. Frank, *J. Am. Chem. Soc.* **2003**, *125*, 6306.
[65] A. Imhof, W. L. Vos, R. Sprik, A. Lagendijk, *Phys. Rev. Lett.* **1999**, *83*, 2942.
[66] X. Chen, J. Ye, S. Ouyang, T. Kako, Z. Li, Z. Zou, *ACS Nano* **2011**, *5*, 4310.
[67] M. Wu, Y. Li, Z. Deng, B. Su, *ChemSusChem* **2011**, *4*, 1481.
[68] J. I. L. Chen, G. A. Ozin, *J. Mater. Chem.* **2009**, *19*, 2675.
[69] Y. Wang, D.-B. Xiong, W. Zhang, H. Su, Q. Liu, J. Gu, S. Zhu, D. Zhang, *Cataly.Today* **2016**, *274*, 15.
[70] O. Deparis, S. R. Mouchet, B. L. Su, *Phys Chem Chem Phys* **2015**, *17*, 30525.
[71] X. Li, X. Zhang, X. Zheng, Y. Shao, M. He, P. Wang, X. Fu, D. Li, *J. Mater. Chem. A* **2015**, *2*, 15976.
[72] R. Mitchell, R. Brydson, R. E. Douthwaite, *Phys Chem Chem Phys* **2015**, *17*, 493.
[73] T. Baba, *Nat. Photon.* **2008**, *2*, 465.
[74] T. F. Krauss, *Nat. Photon.* **2008**, *2*, 448.
[75] V. P. Bykov, *Soviet J. Quantum Elec.* **1975**, *4*, 861.
[76] K. Ohtaka, *Phys. Rev. B* **1979**, *19*, 5057.
[77] E. Yablonovitch, T. Gmitter, K. Leung, *Phys. Rev. Lett.* **1991**, *67*, 2295.
[78] B. T. Holland, C. F. Blanford, A. Stein, *Science* **1998**, *281*, 538.
[79] J. I. Chen, G. von Freymann, S. Y. Choi, V. Kitaev, G. A. Ozin, *Adv. Mater.* **2006**, *18*, 1915.
[80] J. I. Chen, E. Loso, N. Ebrahim, G. A. Ozin, *J. Am. Chem. Soc.* **2008**, *130*, 5420.
[81] M. Zalfani, B. van der Schueren, Z.-Y. Hu, J. C. Rooke, R. Bourguiga, M. Wu, Y. Li, G. Van Tendeloo, B.-L. Su, *J. Mater. Chem. A* **2015**, *3*, 21244.

[82] D. S. Bykov, O. A. Schmidt, T. G. Euser, P. S. J. Russell, *Nat. Photon.* **2015**, *9*, 461.
[83] C. T. Dinh, H. Yen, F. Kleitz, T. O. Do, *Angew. Chem. Int. Ed.* **2014**, *53*, 6618.
[84] M. Deubel, G. von Freymann, M. Wegener, S. Pereira, K. Busch, C. M. Soukoulis, *Nat. Mater.* **2004**, *3*, 444.
[85] N. D. Petkovich, S. G. Rudisill, B. E. Wilson, A. Mukherjee, A. Stein, *Inorg Chem* **2014**, *53*, 1100.
[86] J. Marques-Hueso, R. Peretti, R. Abargues, B. S. Richards, C. Seassal, J. P. Martínez-Pastor, *Adv. Opt. Mater.* **2015**, *3*, 568.
[87] Y. A. Vlasov, K. Luterova, I. Pelant, B. Hönerlage, V. Astratov, *Appl. Phys. Lett.* **1997**, *71*, 1616.
[88] J. I. L. Chen, G. A. Ozin, *Adv. Mater.* **2008**, *20*, 4784.
[89] Y. Wei, J. Jiao, Z. Zhao, J. Liu, J. Li, G. Jiang, Y. Wang, A. Duan, *Appl. Catal. B-Environ.* **2015**, *179*, 422.
[90] M. Wu, J. Jin, J. Liu, Z. Deng, Y. Li, O. Deparis, B.-L. Su, *J. Mater. Chem. A* **2013**, *1*, 15491.
[91] J. Liu, J. Jin, Y. Li, H.-W. Huang, C. Wang, M. Wu, L.-H. Chen, B.-L. Su, *J. Mater. Chem. A* **2014**, *2*, 5051.
[92] H. Tong, S. Ouyang, Y. Bi, N. Umezawa, M. Oshikiri, J. Ye, *Adv. Mater.* **2012**, *24*, 229.
[93] J. I. Chen, G. von Freymann, V. Kitaev, G. A. Ozin, *J. Am. Chem. Soc.* **2007**, *129*, 1196.
[94] Y. Lu, H. Yu, S. Chen, X. Quan, H. Zhao, *Environ. Sci. Technol.* **2012**, *46*, 1724.
[95] X. Zhang, Y. Liu, S.-T. Lee, S. Yang, Z. Kang, *Energy Environ. Sci.* **2014**, *7*, 1409.
[96] L. Zhang, C. Y. Lin, V. K. Valev, E. Reisner, U. Steiner, J. J. Baumberg, *Small* **2014**, *10*, 3970.
[97] Y. Wang, D.-B. Xiong, W. Zhang, H. Su, Q. Liu, J. Gu, S. Zhu, D. Zhang, *Catal. Today* **2016**, *274*, 15.
[98] L. J. Diguna, Q. Shen, J. Kobayashi, T. Toyoda, *Appl. Phys. Lett.* **2007**, *91*, 023116.
[99] A. Mekis, J. C. Chen, I. Kurland, S. Fan, P. R. Villeneuve, J. D. Joannopoulos, *Phys. Rev. Lett.* **1996**, *77*, 3787.
[100] K. Sakoda, M. Sasada, T. Fukushima, A. Yamanaka, N. Kawai, K. Inoue, *JOSA B* **1999**, *16*, 361.
[101] M. Scalora, J. P. Dowling, C. M. Bowden, M. J. Bloemer, *Phys. Rev. Lett.* **1994**, *73*, 1368.
[102] J. P. Dowling, M. Scalora, M. J. Bloemer, C. M. Bowden, *J. Appl. Phys.* **1994**, *75*, 1896.
[103] M. D. Tocci, M. Scalora, M. J. Bloemer, J. P. Dowling, C. M. Bowden, *Phys. Rev. A* **1996**, *53*, 2799.
[104] R. J. Carlson, S. A. Asher, *Appl. Spectrosc.* **1984**, *38*, 297.
[105] P. L. Flaugh, S. E. O'Donnell, S. A. Asher, *Appl. Spectrosc.* **1984**, *38*, 847.
[106] A. Mihi, H. Miguez, *J. Phys. Chem. B* **2005**, *109*, 15968.

[107] Y. Li, F. Piret, T. Léonard, B.-L. Su, *J. Colloid Interface Sci.* **2010**, *348*, 43.
[108] H. Li, J. Wang, Z. Pan, L. Cui, L. Xu, R. Wang, Y. Song, L. Jiang, *J. Mater. Chem.* **2011**, *21*, 1730.
[109] Y. A. Vlasov, V. N. Astratov, A. V. Baryshev, A. A. Kaplyanskii, O. Z. Karimov, M. F. Limonov, *Phys. Rev. E* **2000**, *61*, 5784.
[110] M. Müller, R. Zentel, TMakaorsten , e. G. SRomanov, C. M. S. Torres, *Adv. Mater.* **2000**, *12*, 1499.
[111] S. G. Johnson, J. D. Joannopoulos, *Photonic crystals: the road from theory to practice*, Springer Science & Business Media, 2002.
[112] M. Ren, R. Racikrishna, K. T. Valsaraj, *Environ.Sci.Technol.* **2006**, *40*, 7029.
[113] A. L. Reynolds, U. Peschel, F. Lederer, P. J. Roberts, T. F. Krauss, P. J. I. d. Maagt, *IEEE T. Micorw. Theory* **2001**, *49*, 1860.
[114] J. Léonard, N. Lecong, J.-P. Likforman, O. Crégut, P. Leproux, V. Couderc, S. Haacke, presented at Photonic Crystal Materials and Devices III, Near-UV supercontinua generated in photonic crystal fibers for femtosecond spectroscopy, France, (April,**2006**).
[115] E. Ozbay, *J. Opt. Soc. Am. B* **1996**, *13*, 1945.
[116] S. Lin, J. Fleming, D. Hetherington, B. Smith, R. Biswas, K. Ho, M. Sigalas, W. Zubrzycki, S. Kurtz, J. Bur, *Nature* **1998**, *394*, 251.
[117] J. H. Moon, Y.-S. Cho, S.-M. Yang, *Bull. Korean Chem. Soc.* **2009**, *30*, 2245.
[118] G. M. Gratson, M. Xu, J. A. Lewis, *Nature* **2004**, *428*, 386.
[119] J. H. Moon, S. Yang, *Chem. Rev.* **2009**, *110*, 547.
[120] G. Collins, M. Blomker, M. Osiak, J. Holmes, M. Bredol, C. O'Dwyer, *Chem. Mater.* **2013**, *25*, 4312.
[121] X. Li, H. Dai, J. Deng, Y. Liu, S. Xie, Z. Zhao, Y. Wang, G. Guo, H. Arandiyan, *Chem. Eng. J.* **2013**, *228*, 965.
[122] W. Liu, B. Zou, J. Zhao, H. Cui, *Thin Solid Films* **2010**, *518*, 4923.
[123] G. I. N. Waterhouse, M. R. Waterland, *Polyhedron* **2007**, *26*, 356.
[124] R. M. Almeida, M. Clara Gonçalves, S. Portal, *J. Non-Cryst.Solids* **2004**, *345-346*, 562.
[125] H. Míguez, F. Meseguer, C. López, A. Mifsud, J. S. Moya, L. Vázquez, *Langmuir* **1997**, *13*, 6009.
[126] A. L. Rogach, N. A. Kotov, D. S. Koktysh, J. W. Ostrander, G. A. Ragoisha, *Chem. Mater.* **2000**, *12*, 2721.
[127] J. F. B. P. Jiang, K. S. Hwang, and V. L. Colvin, *Chem. Mater.* **1999**, *11*, 2132.
[128] S. M. Yang, G. A. Ozin, *Chem. Commun.* **2000**, *24*, 2507.
[129] A. Imhof, D. J. Pine, *Nature* **1997**, *389*, 948.
[130] A. Blanco, E. Chomski, S. Grabtchak, M. Ibisate, S. John, S. W. Leonard, C. Lopez, F. Meseguer, H. Miguez, J. P. Mondia, G. A. Ozin, O. Toader, H. M. van Driel, *Nature* **2000**, *405*, 437.
[131] H. Yan, C. F. Blanford, B. T. Holland, W. H. Smyrl, A. Stein, *Chem.Mater.* **2000**, *12*, 1134.

[132] B. Hatton, L. Mishchenko, S. Davis, K. H. Sandhage, J. Aizenberg, *PANS* **2010**, *107*, 10354.
[133] B. H. Juárez, P. D. García, D. Golmayo, A. Blanco, C. López, *Adv. Mater.* **2005**, *17*, 2761.
[134] J. S. King, E. Graugnard, C. J. Summers, *Adv. Mater.* **2005**, *17*, 1010.
[135] A. Stein, N. R. Denny, *Chem. Mater.* **2008**, *20*, 649.
[136] P. V. Braun, P. Wiltzius, *Nature* **1999**, *402*, 603.
[137] Y. Huang, C. Liao, B. Huang, W. Chen, P. Wu, *J. Electrochem. Soc.* **2011**, *158*, 45.
[138] Y. Valsov, X. Bo, J. C.Sturm, D. J.Norris, *Nature* **2001**, *414*, 289.
[139] J. D. Joannopoulos, P. R. Villeneuve, S. Fan, *Nature* **1997**, *386*, 143.
[140] A. Mihi, H. Míguez, *J. Phys. Chem. B* **2005**, *109*, 15968.
[141] J. I. Chen, G. A. Ozin, *Adv. Mater.* **2008**, *20*, 4784.
[142] Z. Cai, Z. Xiong, X. Lu, J. Teng, *J. Mater. Chem. A* **2014**, *2*, 545.
[143] Z. Zhang, L. Zhang, M. N. Hedhili, H. Zhang, P. Wang, *Nano Lett.* **2012**, *13*, 14.
[144] S. Guldin, S. Huttner, M. Kolle, M. E. Welland, P. Muller-Buschbaum, R. H. Friend, U. Steiner, N. Tetreault, *Nano Lett.* **2010**, *10*, 2303.
[145] T. Suezaki, H. Yano, T. Hatayama, G. A. Ozin, T. Fuyuki, *Appl. Phys. Lett.* **2011**, *98*, 072106.
[146] S. Bayram, L. Halaoui, *Part. Part. Syst. Chara.* **2013**, *30*, 706.
[147] J. Xiao, Q. Huang, J. Xu, C. Li, G. Chen, Y. Luo, D. Li, Q. Meng, *J. Phys. Chem. C* **2014**, *118*, 4007.
[148] A. Mihi, M. E. Calvo, J. Anta, H. Miguez, *J. Phys. Chem. Lett.* **2008**, *112*, 13.
[149] C. Peng, Y. Liang, K. Sakai, S. Iwahashi, S. Noda, *Opt. Express* **2011**, *19*, 24672.
[150] S. Noda, *Science* **2001**, *293*, 1123.
[151] Y. Liang, C. Peng, K. Ishizaki, S. Iwahashi, K. Sakai, Y. Tanaka, K. Kitamura, S. Noda, *Opt. Express* **2013**, *21*, 565.
[152] H. Benisty, S. Olivier, M. Rattier, C. Weisbuch, *Applications of two-dimensional photonic crystals to semiconductor optoelectronic devices*, Vol. 563, Springer Netherlands, Germany **2001**.
[153] H. Li, D. Ma, C. Yang, Y. Xu, Z. Liu, *Opt. Express* **2012**, *20*, 24342.
[154] E. Matioli, S. Keller, F. Wu, Y.-S. Choi, E. Hu, J. Speck, C. Weisbuch, *J. Appl. Phys.* **2009**, *106*, 024309.
[155] P. N. Patel, V. Mishra, in *Emerging Technology Trends in Electronics, Communication and Networking (ET2ECN), 2012 1st International Conference on. IEEE*, IEEE, 2012, 1.
[156] C. T. Dinh, H. Yen, F. Kleitz, T. O. Do, *Angew. Chem. Int. Ed.* **2014**, *53*, 6618.
[157] M. Wu, J. Liu, J. Jin, C. Wang, S. Huang, Z. Deng, Y. Li, B.-L. Su, *Appl. Catal. B* **2014**, *150-151*, 411.

[158] J. Liu, G. Liu, M. Li, W. Shen, Z. Liu, J. Wang, J. Zhao, L. Jiang, Y. Song, *Energy Environ. Sci.* **2010**, *3*, 1503.
[159] Shin-ichi Naya, Aimi Inoue, H. Tada, *J. Am. Chem. Soc.* **2010**, *132*, 6292.
[160] H. Xie, Y. Li, S. Jin, J. Han, X. Zhao, *J. Phys. Chem. C* **2010**, *114*, 9706.
[161] S. L. Chen, A. J. Wang, C. T. Hu, C. Dai, J. B. Benziger, *AIChE Journal* **2012**, *58*, 568.
[162] C. Li, X. Zhu, H. Zhang, Z. Zhu, B. Liu, C. Cheng, *Adv. Mater. Interfaces* **2015**, *2*, 1500428.
[163] C. Aprile, A. Corma, H. Garcia, *Phys Chem Chem Phys* **2008**, *10*, 769.
[164] J. I. L. Chen, G. von Freymann, S. Y. Choi, V. Kitaev, G. A. Ozin, *J. Mater. Chem.* **2008**, *18*, 369.
[165] A. Mihi, H. Míguez, I. Rodríguez, S. Rubio, F. Meseguer, *Phys. Rev. B* **2005**, *71*, 1251311.
[166] A. Kudo, Y. Miseki, *Chem Soc Rev* **2009**, *38*, 253.
[167] S. Lam, J. Sin, A. Z. Abdullah, A. R. Mohamed, *Desalin.Water Treat.* **2012**, *41*, 131.
[168] S. Khanchandani, S. Kundu, A. Patra, A. K. Ganguli, *J. Phys. Chem. C* **2012**, *116*, 23653.
[169] C. M. Janet, S. Navaladian, B. Viswanathan, T. K. Varadarajan, R. P. Viswanath, *J. Phys. Chem. C* **2010**, *114*, 2622.
[170] S. Meng, D. Li, P. Wang, X. Zheng, J. Wang, J. Chen, J. Fang, X. Fu, *RSC Advances* **2013**, *3*, 17021.
[171] X. Chen, S. Shen, L. Guo, S. S. Mao, *Chem. Rev.* **2010**, *110*, 6503.
[172] L. Zhang, H. H. Mohamed, R. Dillert, D. Bahnemann, *J. Photoch. Photobio.C* **2012**, *13*, 263.
[173] Y. Wei, J. Jiao, Z. Zhao, J. Liu, J. Li, G. Jiang, Y. Wang, A. Duan, *Appl. Catal.B: Environ.* **2015**, *179*, 422.
[174] (a) M. Zalfani, B. van der Schueren, M. Mahdouani, R. Bourguiga, W.-B. Yu, M. Wu, O. Deparis, Y. Li, B.-L. Su, *Appl. Catal.B: Environ.* **2016**, *199*, 187. (b) M. Zalfani, Z. Deng, M. Mahdouani, R. Bourguiga, M. Wu, Y. Li, B.-L. Su, *Appl. Catal.B: Environ.* **2017**, *in press*
[175] T. Suezaki, P. G. O'Brien, J. I. Chen, E. Loso, N. P. Kherani, G. A. Ozin, *Adv. Mater.* **2009**, *21*, 559.
[176] Y. L. Lee, Y. S. Lo, *Adv. Funct. Mater.* **2009**, *19*, 604.
[177] T. Suezaki, J. I. L. Chen, T. Hatayama, T. Fuyuki, G. A. Ozin, *Appl. Phys. Lett.* **2010**, *96*, 242102.
[178] S. Colodrero, A. Mihi, L. Häggman, M. Ocana, G. Boschloo, A. Hagfeldt, H. Miguez, *Adv. Mater.* **2009**, *21*, 764.
[179] T. Toyoda, Q. Shen, *J Phys Chem Lett* **2012**, *3*, 1885.
[180] M. Grätzel, *Comptes Rendus Chimie* **2006**, *9*, 578.
[181] M. Grätzel, *J. Photoch. Photobio.C* **2003**, *4*, 145.
[182] K. Sakoda, *Opt. Express* **1999**, *4*, 167.
[183] D. M. Mittleman, J. F. Bertone, P. Jiang, K. S. Hwang, V. L. Colvin, *J. Chem. Phys.* **1999**, *111*, 345.

[184] R. Rengarajan, D. Mittleman, C. Rich, V. Colvin, *Phys. Rev. E* **2005**, *71*, 0166151.
[185] Maysaa El Harakeh, L. Halaoui, *J. Phys. Chem. C* **2010**, *114*, 2806.
[186] J. Zhou, H. Li, L. Ye, J. Liu, J. Wang, T. Zhao, L. Jiang, Y. Song, *J. Phys. Chem. C* **2010**, *114*, 22303.
[187] Y. A. Vlasov, M. A. Kaliteevski, V. V. Nikolaev, *Phys. Rev. B* **1999**, *60*, 1555.
[188] Y. A. Vlasov, V. N. Astratov, O. Z. Karimov, A. A. Kaplyanskii, V. N. Bogomolov, A. V. Prokofiev, *Phys. Rev. B* **1997**, *55*, 133571.
[189] J. Galisteo-López, E. Palacios-Lidón, E. Castillo-Martinez, C. López, *Phys. Rev. B* **2003**, *68*, 115109.
[190] T. G. Euser, A. J. Molenaar, J. G. Fleming, B. Gralak, A. Polman, W. L. Vos, *Phys. Rev. B* **2008**, *77*.
[191] D. Schneider, F. Liaqat, H. El Boudouti el, Y. El Hassouani, B. Djafari-Rouhani, W. Tremel, H. J. Butt, G. Fytas, *Nano Lett.* **2012**, *12*, 3101.
[192] I. Pavlichenko, A. T. Exner, M. Guehl, P. Lugli, G. Scarpa, B. V. Lotsch, *J. Phys. Chem. C* **2012**, *116*, 298.
[193] Z. Wu, D. Lee, M. F. Rubner, R. E. Cohen, *Small* **2007**, *3*, 1445.
[194] S. Colodrero, M. Ocaña, H. Míguez, *Langmuir* **2008**, *24*, 4430.
[195] S. Y. Choi, M. Mamak, G. v. Freymann, N. Chopra, G. A. Ozin, *Nano Lett.* **2006**, *6*, 2456.
[196] D. L. Guo, L. X. Fan, F. H. Wang, S. Huang, X. Zou, *J. Phys. Chem. C* **2008**, *112*, 17952.
[197] J. Jiao, Y. Wei, Z. Zhao, W. Zhong, J. Liu, J. Li, A. Duan, G. Jiang, *Catal. Today* **2015**, *258*, 319.
[198] C. Fenzl, C. Genslein, A. Zöpfl, A. J. Baeumner, T. Hirsch, *J. Mater. Chem. B* **2015**, *3*, 2089.
[199] C. O. R. Quiroz, I. Levchuk, C. Bronnbauer, M. Salvador, K. Forberich, T. Heumüller, Y. Hou, P. Schweizer, E. Spiecker, C. J. Brabec, *J. Mater. Chem. A* **2015**, *3*, 24071.
[200] B. Rafael, R.-G. Pablo, M.-O. Alberto, E. Xavier, M. Marc, M. Jordi, *Nat. Photon.* **2013**, *7*, 995.
[201] Y. Zhang, Z. Peng, C. Cai, Z. Liu, Y. Lin, W. Zheng, J. Yang, L. Hou, Y. Cao, *J. Mater. Chem. A* **2016**, *4*, 11821.
[202] R. R. Lunt, V. Bulovic, *Appl. Phys. Lett.* **2011**, *98*, 113305.

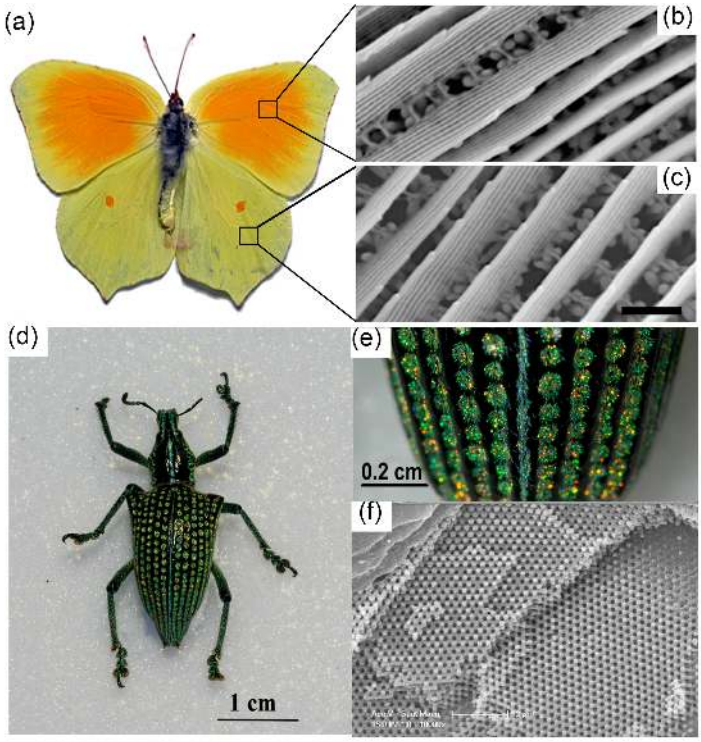

Figure 1. Photograph (a), Scanning Electron Microscope (SEM) images of the forewing (b) and hindwing (c) of *G Cleopatra* butterfly (scale bar 1 μ m) [55] (Copyright 2011, Springer).; Photograph (d), optical microscope (e) and SEM image (f) of the Brazilian weevil *E. imperialis* [54] (Copyright 2010, Elsevier Science SA).

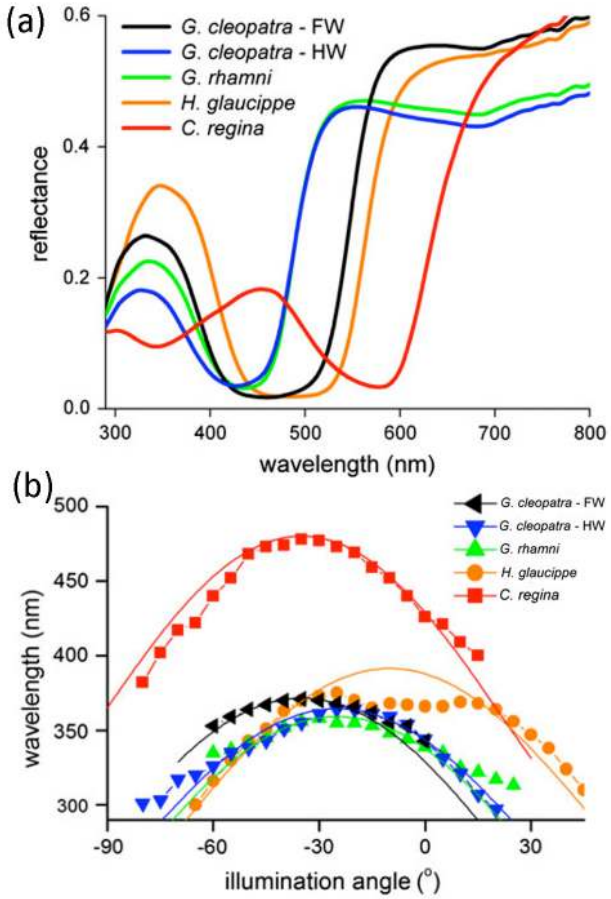

Figure 2. Reflectance spectra of the iridescent wing areas of four butterfly species (*G. cleopatra*, *G. rhamni*, *H. glaucippe*, *C. regina*) measured with an integrating sphere (FW: forewing, HW: hindwing (a); Peak wavelength of the iridescence band as a function of angle of incidence, with negative angles signifying a tilt of the ridge multilayers towards the wing base. (b)[55] (Copyright 2011, Springer).

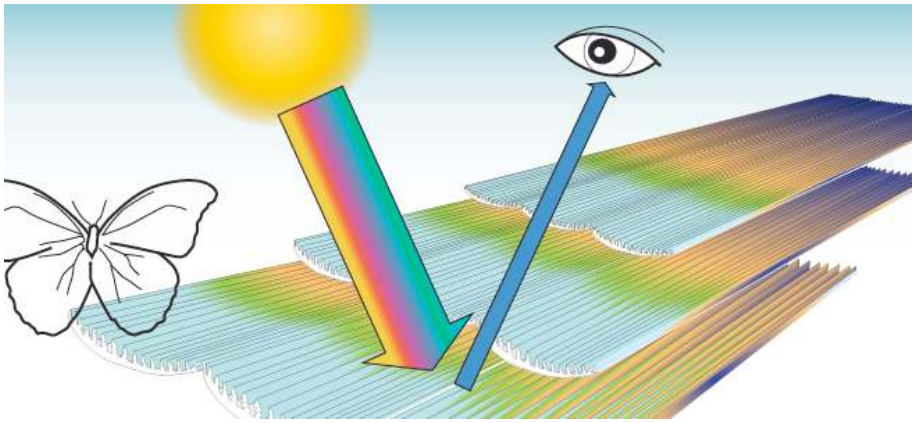

Figure 3. Illustrations showing wings of Morpho butterflies which create blue color upon reflection of visible light by diffracting and scattering it[63]

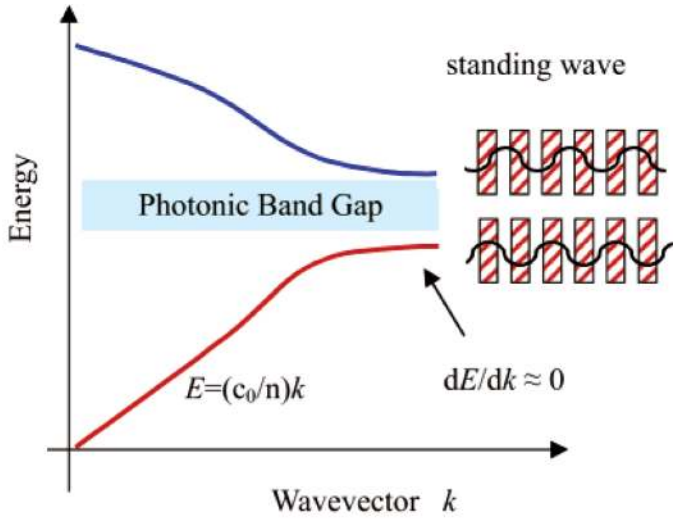

Figure 4. Simplified photonic band structure of a photonic crystal[64]. Near the Brillouin zone, center light travels with velocity c_0/n, where c_0 is the speed of light in a vacuum, and n is the average refractive index. At photon energies approaching a full band gap or stop band from the red side, the group velocity of light decreases and light can be increasingly described as a sinusoidal standing wave that has its highest amplitude in the high refractive index part of the structure. At energies above the band gap or stop band, the standing wave is predominantly localized in the low index part of the photonic crystal, i.e., in the air voids. (Copyright 2003, the American Chemical Society).

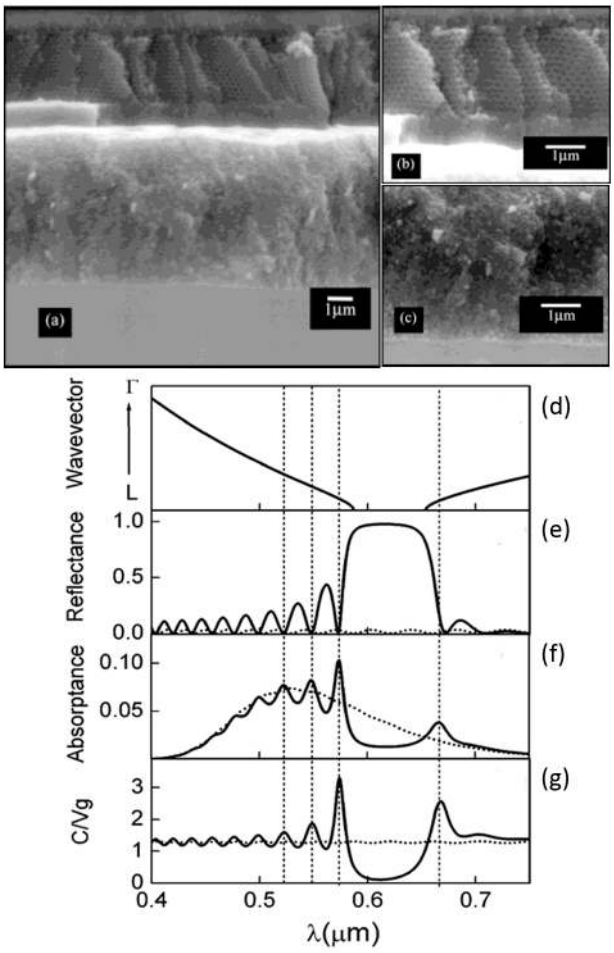

Figure 5. (a-c)SEM images of bilayer photonic crystal-nano TiO_2 photoeletrode extracted from ref [64], (d) Calculated photonic band structure along the Γ-L direction for a close-packed fcc titania inverse opal; (e) reflectance, (f) absorbance and (g) ratio between light speed in vacuum (*c*) and group velocity (V_g) for a slab of titania inverse opal (solid lines) and a non-structured slab with same thickness and amount of absorbing materials (dashed lines).[106] (Copyright 2005, American Chemical Society).

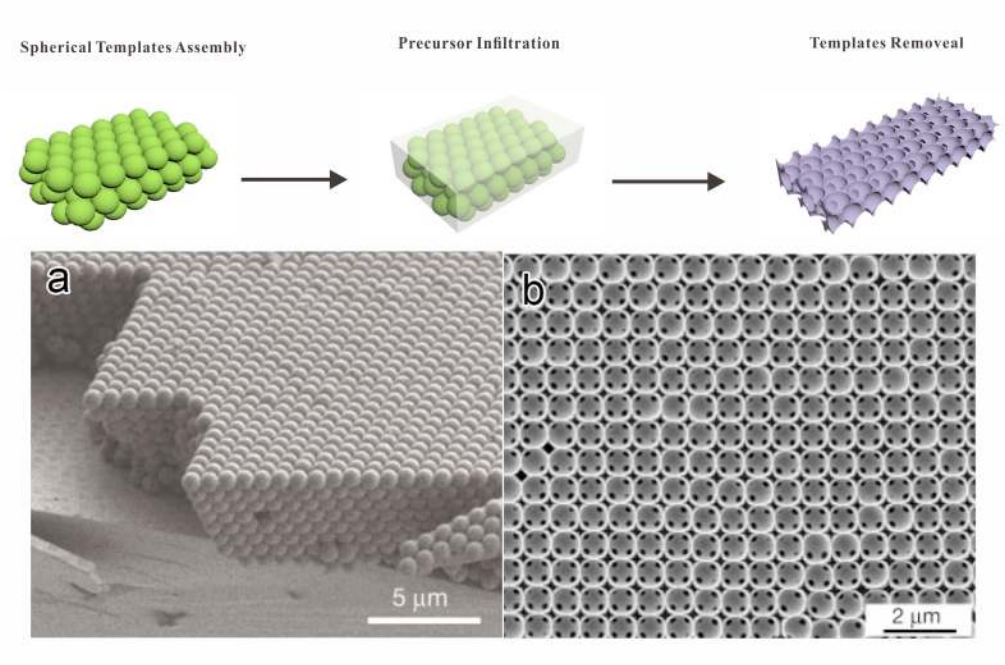

Figure 6. Schematic processes for the synthesis of inverse opals and cross-sectional SEM images of silica opal (a) and silica-based inverse opal (b)[138]. (Copyright 2001, Nature).

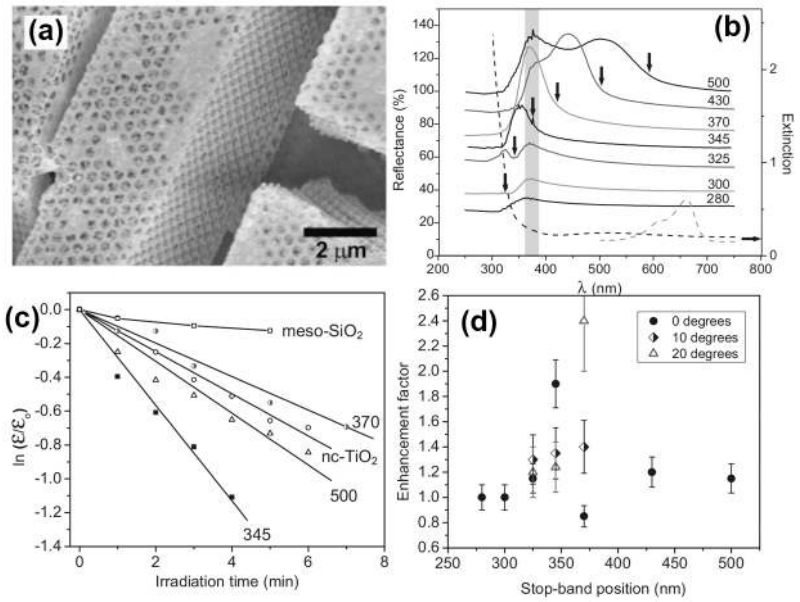

Figure 7. (a) SEM image of TiO_2 inverse opal; (b) Reflectance spectra of TiO_2 inverse opals with different pore sizes along with the extinction spectra of nanocrystalline TiO_2 (black dashed line) and methylene blue (gray dashed line). The shaded area is the monochromatic irradiation wavelength used in the photocatalysis experiments; (c) Photodegradation rate plot for TiO_2 inverse opals with stop band maximum at 345 nm, 370 nm and 500 nm under 370 ±10 nm irradiation. Mesoporous SiO_2 was used as a blank for comparison; (d) Photoactivity enhancement factor for all TiO_2 inverse opals versus the stopband (i.e. photonic band gap) position under the same monochromatic irradiation wavelength, showing strong angular dependency[79]. (Copyright 2006, Wiley-VCH).

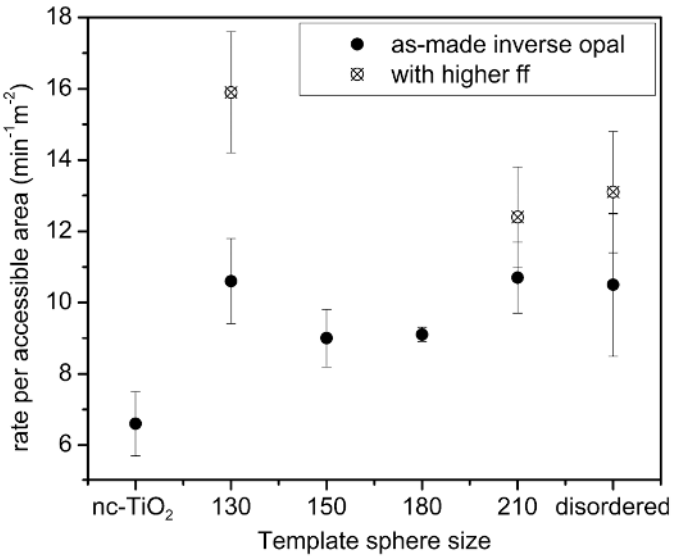

Figure 8. Normalized first-order decay rate constant of liquid phase (dye solution) photocatalysis as function of the dye accessible area for different films: nanocrystalline TiO_2, TiO_2 inverse opal and TiO_2 inverse opal with TiF_6^{2-} treatment to increase titania wall thickness[68]. (Copyright 2009, Royal Society Chemistry).

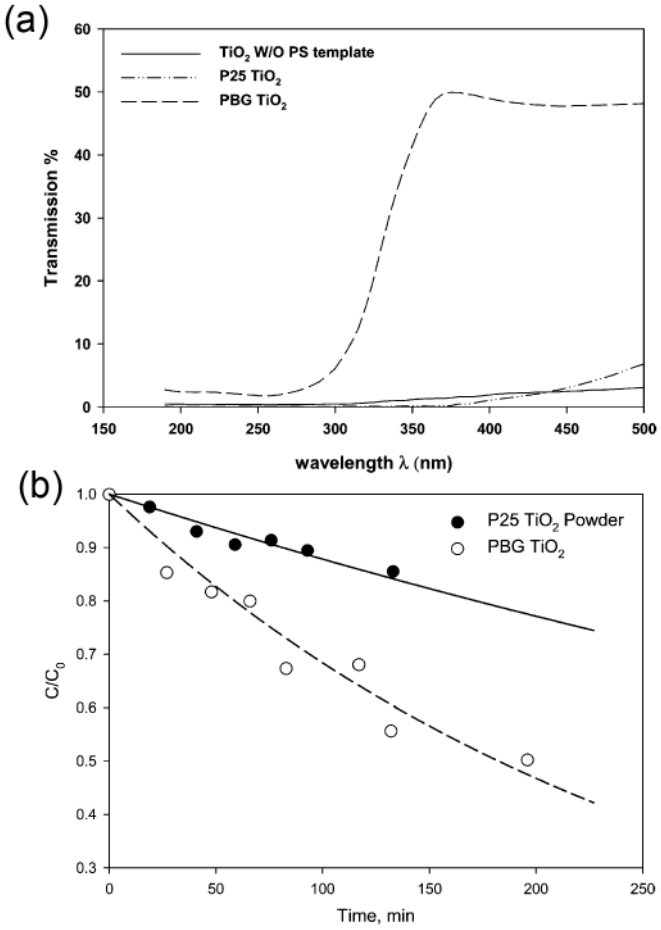

Figure 9. (a) Transmission spectra of TiO_2 without photonic structure (TiO_2 W/O PS template), TiO_2 inverse opal (PBG-TiO_2) and commercial P25 TiO_2; (b) Normalized concentrations of 1,2-dichlorobenzene as a function of the irradiation time in the presence of P25 TiO_2 powder (closed circles) or TiO_2 inverse opal (PBG TiO_2, open circles) showing the higher activity of PBG-TiO_2[112]. (Copyright 2006, American Chemical Society).

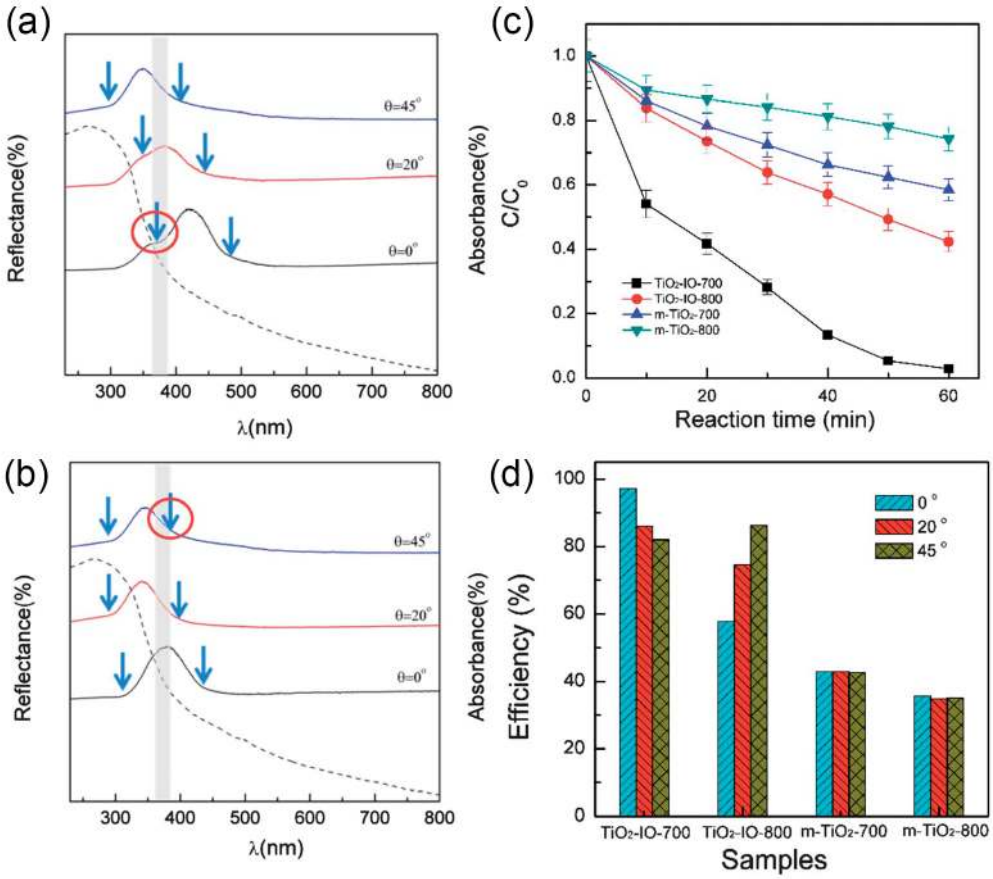

Figure 10. Reflectance spectra of TiO_2-IO-700 (a) and TiO_2-IO-800 (b) films measured in water, showing the variation of the photonic band gap position (reflectance peak) at different light incidence angles ($\theta = 0°$, $\theta = 20°$ and $\theta = 45°$). The shaded region indicates the electronic absorption band edge of TiO_2. The absorbance spectrum of TiO_2-IO is shown in black dashed line. Arrows show the positions of red edge and blue edge of the PBG. (c) Photodegradation rate of RhB solution on TiO_2-IO-films ($\theta = 0°$). (d) Photodegradation rate of RhB on TiO_2-IO films ($\theta = 0°$, $\theta = 20°$ and $\theta = 45°$) and mesoporous TiO_2 films ($\theta = 0°$). All the samples were calcinated at 700 ° and 800 °C, respectively[90]. (Copyright 2013, Royal Society Chemistry).

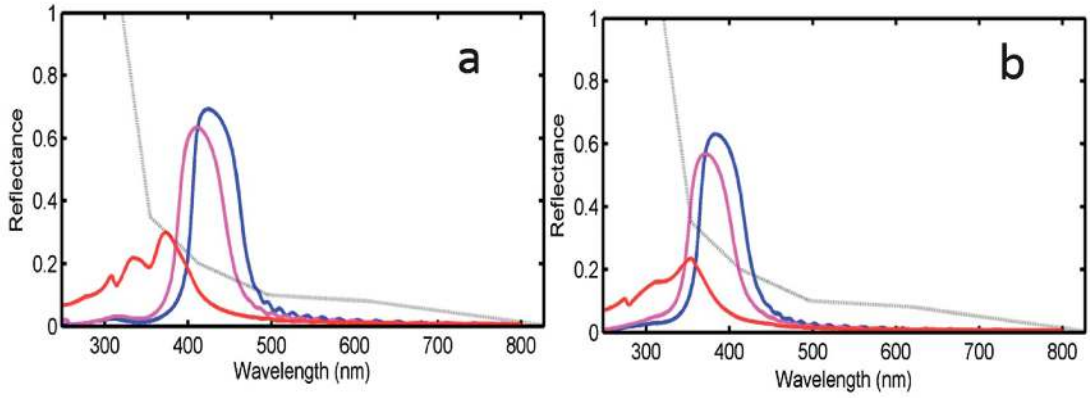

Figure 11. Theoretical reflectance spectra of water immersed TiO_2 inverse opal films on quartz substrate (a): D=185 nm, (b): D=165 nm for (111) crystal orientation at incidence angles equal to 0° (blue), 20° (magenta) and 45°(red): 5134 nm (a) and 4579 nm (b)[90] (Copyright 2013, Royal Society Chemistry).

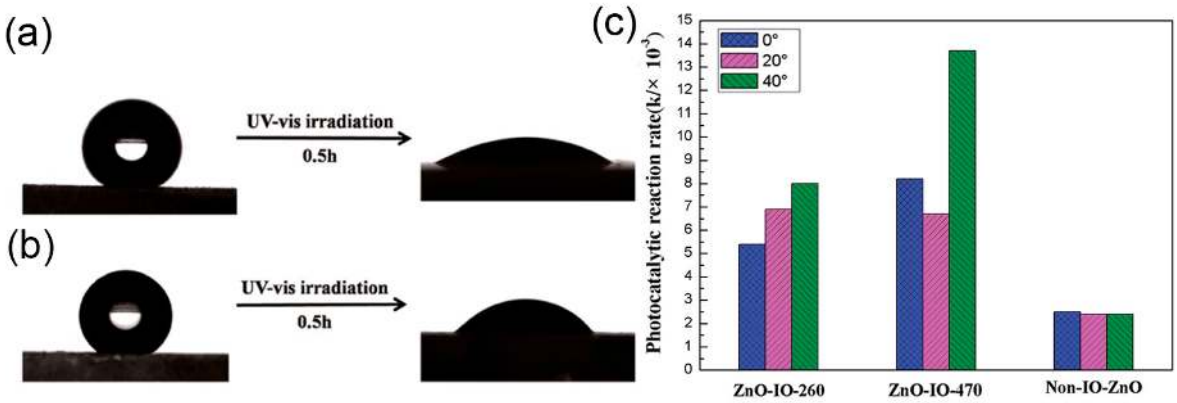

Figure 12. Photographs of water droplet shape on ZnO-IO films using templates with diameter of 260nm and 470nm (abbreviated as ZnO-IO-260 and ZnO-IO-470) before and after UV-vis irradiation for 0.5 h: (a) ZnO-IO-260; (b) ZnO-IO-470; (c) photocatalytic reaction rates of ZnO-IO films and ZnO films without IO nanostructure(abbreviated as non-structured IO film at different incidence angles[91]. (Copyright 2014, Royal Society Chemistry).

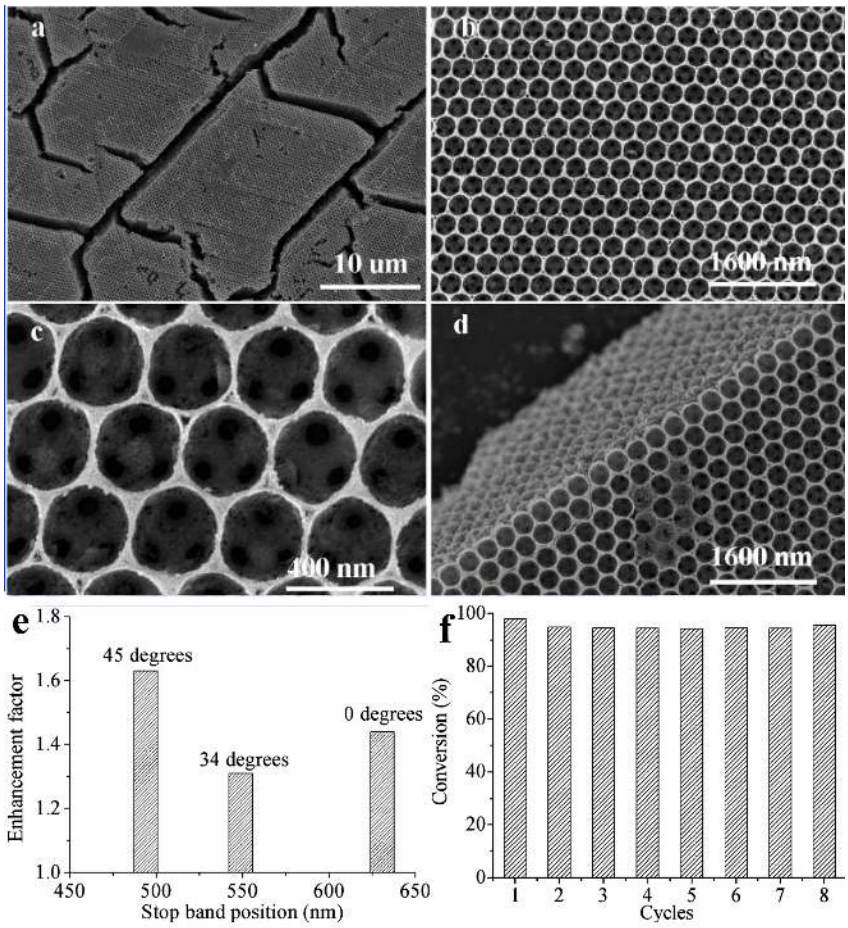

Figure 13. (a-b)SEM images of the 3D-Fe_2O_3 film; (c) photoactivity enhancement factor for 3D-Fe_2O_3 film as a function of stop band (i.e. photonic band gap) position under monochromatic irradiation (550nm) as different angles off-normal of the film;(d) durability of the 3D-Fe_2O_3 film for photodegradation of crystal violet under visible irradiation[160]. (Copyright 2010, American Chemical Society).

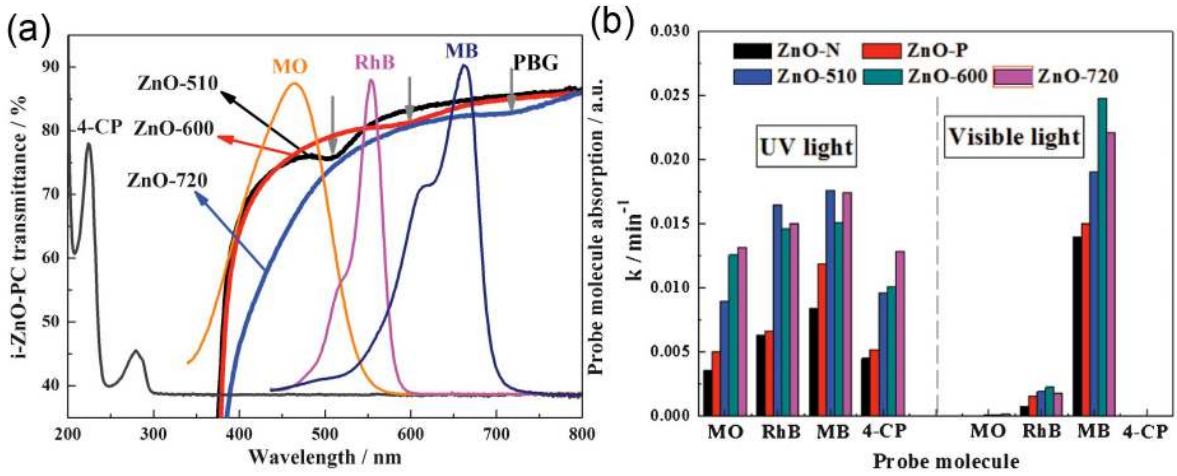

Figure 14. (a) Absorption spectra of the probe molecules and transmittance spectra of ZnO inverse opals. (b) Reaction rate constant of photocatalytic degradation of the probe molecules under UV (left) and visible light (right) irradiation[170]. (Copyright 2013, Royal Society Chemistry).

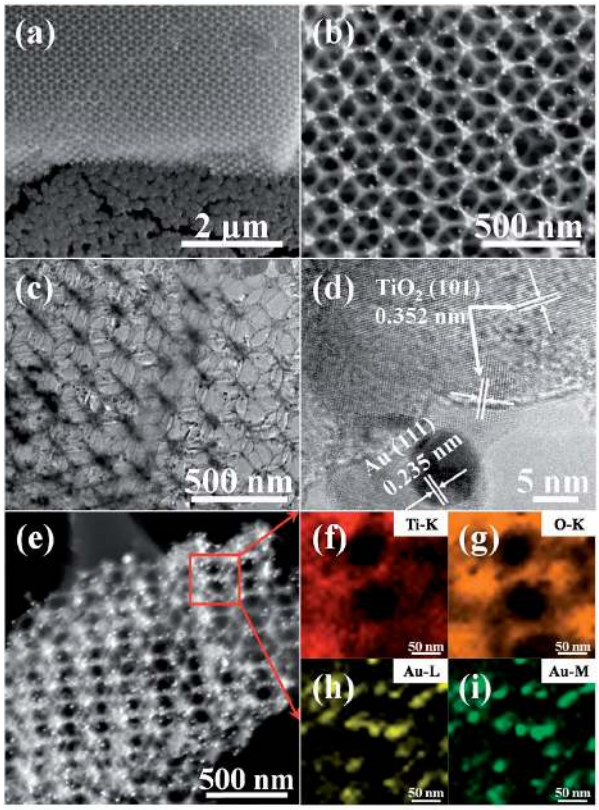

Figure 15. (a) Low-magnification and (b) high-resolution SEM images of Au/TiO_2NRPC structures on the FTO substrate. (c) Low-magnification and (d) high resolution TEM images of Au/TiO_2NRPCs peeled from the FTO substrate. (e) STEM image of Au/TiO_2 NRPCs. (f–i) EDS element mapping images of Ti, O, and Au from the selected area marked with red lines in (e)[95]. (Copyright 2014, Royal Society Chemistry).

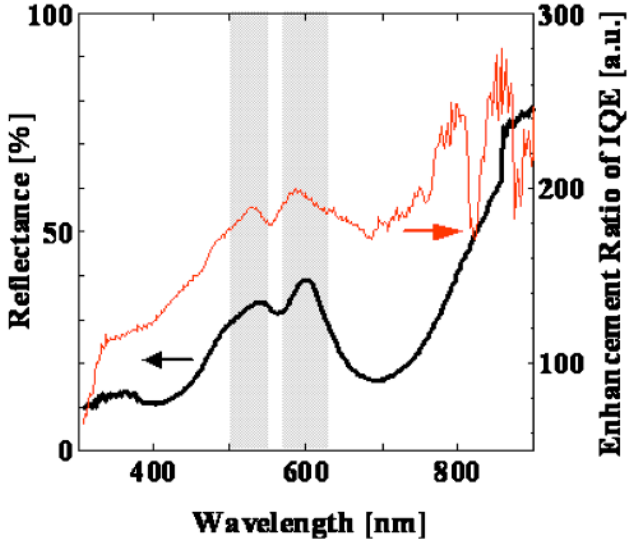

Figure 16. Spectrum of the IQE enhancement (due to HPP post-treatment) ratio for an i-cSi-o structure made from 280 nm spheres and the corresponding reflectance spectrum. The shaded wavelength areas are the observed photonic bandgaps and their peripheral band edges[145]. (Copyright 2011, Applied Physics Letters).

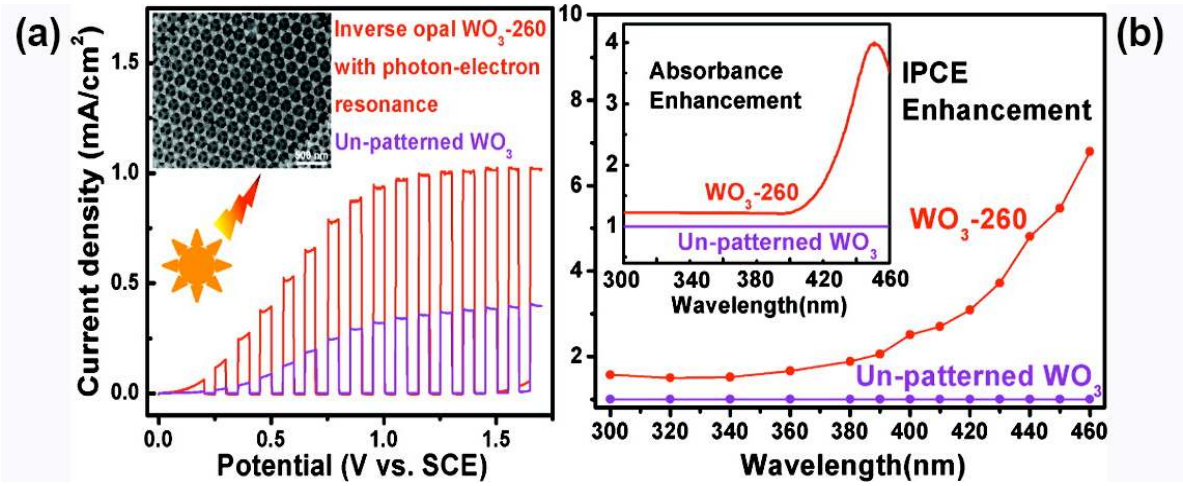

Figure 17. Photocurrent potential curves of WO_3 inverse opals with template diameters of 260 (WO_3-260) and un-patterned WO_3 measured under visible light irradiation ($\lambda > 400$ nm) (the inset image is the SEM images of WO_3-260) (a) IPCE enhancement of WO_3-260 and un-patterned WO_3 as a function of the wavelength (the inset image is the absorbance enhancement of WO_3-260 and un-patterned WO_3)[66]. (Copyright 2011, American Chemical Society).

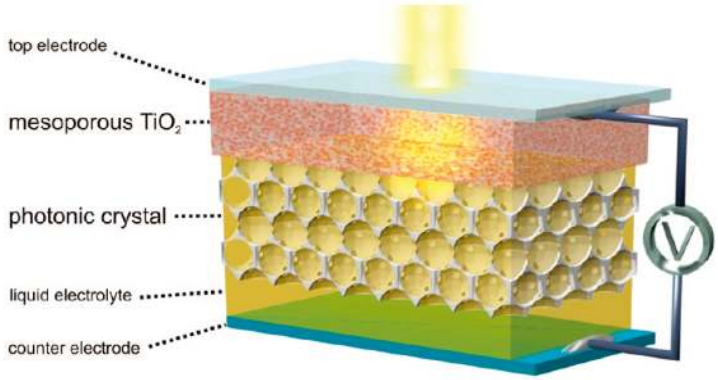

Figure 18. Cross-section of a photonic crystal dye-sensitized solar cell[144]. (Copyright 2010, American Chemical Society).

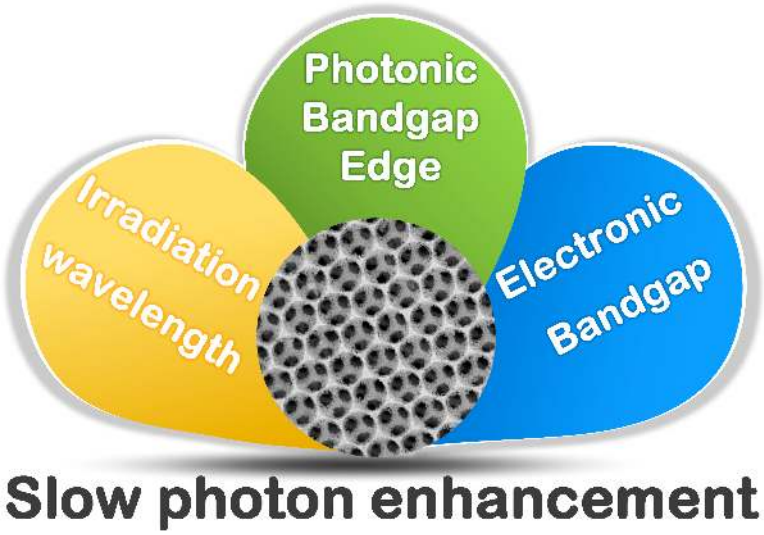

Figure 19. Three phenomena that require coordination for efficient exploitation of slow photons.

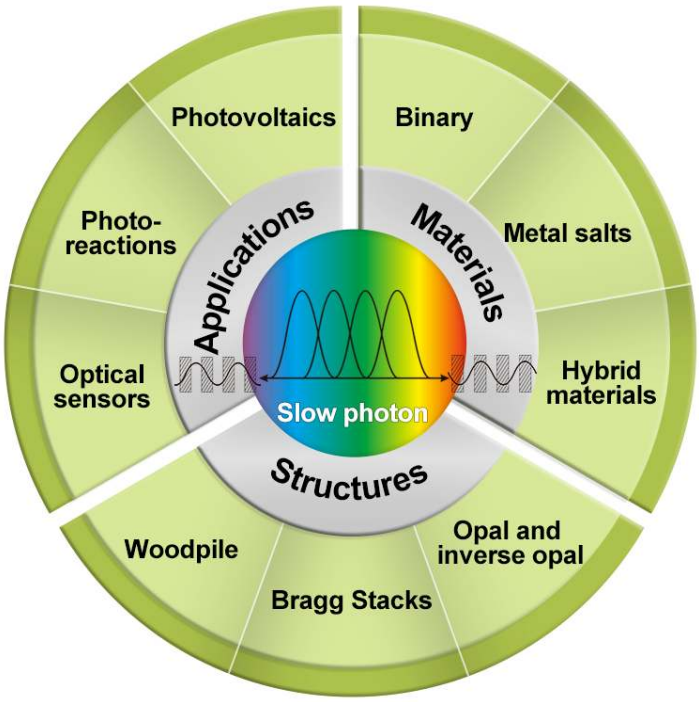

Figure 20. Illustration of the next research and development directions of slow photons.

Slow photons can dramatically enhance the photoreactivity of semiconducting materials. It is believed that "slow photons" will break new ground to improve light harvesting of various materials for all solar-related applications in the future.

Keyword : Photonic Crystal, Slow Photon, Photocatalysis, Photovoltaics

Jing Liu [a], Heng Zhao [a], Benoit Van der Schueren [b], Min Wu [a],*, Yu Li [a], Olivier Deparis [c] , Jinhua Ye [d], Geoffrey Ozin [e], Tawfique Hasan [f] and Bao-Lian Su [a, b,g]*

Title: Slow Photons for Photocatalysis and Photovoltaics

ToC figure :